Quaternary Science Reviews 255 (2021) 106815

Contents lists available at ScienceDirect

Quaternary Science Reviews

journal homepage: www.elsevier.com/locate/quascirev

Last Lateglacial glacier advance in the Gran Paradiso Group reveals relatively drier climatic conditions established in the Western Alps since at least the Younger Dryas

Carlo Baroni [a, b], Simona Gennaro [a], Maria Cristina Salvatore [a, b, *], Susan Ivy-Ochs [c], Marcus Christl [c], Riccardo Cerrato [a], Giuseppe Orombelli [d]

[a] Dipartimento di Scienze della Terra, University of Pisa, Via S. Maria 53, 56126, Pisa, Italy
[b] Istituto di Geoscienze e Georisorse, Consiglio Nazionale delle Ricerche, Pisa, Italy
[c] Laboratory of Ion Beam Physics, ETH Zürich, Switzerland
[d] Dipartimento di Scienze dell'Ambiente e della Terra, University of Milano-Bicocca, Piazza della Scienza 1, 20126, Milano, Italy

ARTICLE INFO

Article history:
Received 30 August 2020
Received in revised form
11 January 2021
Accepted 15 January 2021
Available online xxx

Handling Editor: Dr C. O'Cofaigh

Keywords:
Glacial geomorphology
Paleoclimatology
ELA
Surface Exposure Dating
Cosmogenic ^{10}Be
Late Pleistocene
Younger Dryas
Western Alps

ABSTRACT

The Late Pleistocene to Holocene transition in the Northern Hemisphere was characterized by abrupt millennial-scale climatic changes testified in the Alpine Chain by proxy records derived from glacial landforms and deposits. A detailed reconstruction of the paleo-glaciers during the deposition of the pre-Little Ice Age (LIA) moraines and newly obtained ^{10}Be exposure ages provide information on the timing of a glacier advance in the Gran Paradiso Group (Western Alps, Italy) related to the regional Egesen stadial as a response to the climatic deterioration at around 12.9–11.7 ka (corresponding to the Younger Dryas in northern Europe and to the Greenland stadial 1 in the INTIMATE event stratigraphy). The study area represents a key site to define the behaviour of the Egesen paleo-glaciers, since they are located in a significant climatic area between the moister Maritime Alps and the Northern Alps. The ELA reconstructions and the comparison with other Alpine sectors provide evidence that current relatively drier conditions in the area postdate the LGM and were already present during the Egesen stadial. Our results support a strong positive YD Arctic Oscillation index, which led to drier conditions in southern Europe and caused negative winter precipitation anomalies.

1. Introduction

Alpine glaciers are among the most significant proxies that can be used to understand recent and long-term climate changes, owing to their sensitivity to local and regional climatic conditions. Glacier mass balance is indeed strictly correlated to the climate affecting the area hosting the glacier, although non-climatic factors, such as topography or aspect, may also play an important role in the glacier's variations (Oerlemans, 2001; IPCC, 2007, 2013; Mackintosh et al., 2017). Changes in mass balance determine modifications in glacier extent, thickness and morphology, so that glacier activity may sculpt the landscape and deposit glacial drifts and moraines. Therefore, glacial landforms and deposits of different stadials are powerful tools for reconstructing past glacier extension and paleo-glacier topography which, in turn, are necessary to quantitatively reconstruct past glaciological parameters (i.e. Equilibrium Line Altitude -ELA-, and ELA variation -ΔELA-; Porter, 1975; Porter and Orombelli, 1982).

Chronological constraining of glacial geomorphological features improves the knowledge of Alpine environmental dynamics by ascribing the interested features not only to the main stadials but make it possible to identify and characterize even sub-stadial phases (Ivy-Ochs et al., 2009). Indeed, a better defined chronological control of past glacial phases will render more significant the glaciological parameters obtained for the reconstruction of past climatic changes (Lowe et al., 2008; Rasmussen et al., 2014), suitable to assess the impact of present climate warming. Moreover, the wider and more significant the areas studied, the more noticeable will be the quantitative data obtained.

* Corresponding author. Dipartimento di Scienze della Terra, University of Pisa, Via S. Maria 53, 56126, Pisa, Italy.
E-mail address: mariacristina.salvatore@unipi.it (M.C. Salvatore).

https://doi.org/10.1016/j.quascirev.2021.106815

The last major Lateglacial glacier re-advance phase in the Alps, commonly referred to the Egesen stadial, was a response to the last climatic downturn occurred during the Late Pleistocene at around 12.9 ka, as evidenced elsewhere (e.g. Heuberger, 1968; Kerschner, 1980; Maisch, 1982; Kerschner et al., 2000; Ivy-Ochs et al., 2006, 2008, 2009; Federici et al., 2008, 2017; Heiri et al., 2014b; Rasmussen et al., 2014; Baroni et al., 2014, 2017; Reitner et al., 2016; Boxleitner et al., 2019a, b; Protin et al., 2019).

Although the YD cooling event in the Northern Hemisphere is well testified and supported by numerous climatic reconstructions based on proxies and on modelling, the processes which led to this cold phase and to the abrupt temperature increase that characterized the Pleistocene-Holocene boundary are still not fully understood (Brauer et al., 2008; Broecker et al., 2010; Heiri et al., 2011; Rasmussen et al., 2014; Schenk et al., 2018; Palacios et al., 2020). The precise timing of the YD and the quantitative data on paleo-ELAs and on their fluctuations are fundamental tools to infer the paleo-climatic parameters able to produce glacier mass balance changes, reflected by modification of their extent and shape. Understanding the reaction of the Alpine glacier to abrupt naturally-driven past climatic changes represents a key point for the modelling of glacier reactions to ongoing and future climatic and environmental changes.

Recent studies in the Rhaetian and Maritime Italian Alps, geomorphological interpretations and radiometric ages have supplied information on glacier quantitative parameters (i.e., areas, volumes, paleo-ELAs and ΔELAs) and their timing during the last Lateglacial interstadial (Moran et al., 2016; Baroni et al., 2017; Federici et al., 2017; Spagnolo and Ribolini, 2019). However, there is an evident paucity of data concerning the Graian Italian Alps, where the Gran Paradiso Group is hosted, an important climatic hinge between the Mediterranean Basin and the Central Alps (Crespi et al., 2018). Indeed, previous studies (Sacco, 1921a, 1921b, 1925; Beschel, 1958; Mortara et al., 1992) have analysed glacial landforms located downvalley from the Little Ice Age (LIA) moraines, arguing that they may have developed during Lateglacial advance phases. To date, there are no data available about quantitative data on spatial and temporal extent variability of the paleo-glacier nor about the ELA, despite the inclusion of the Gran Paradiso in a complex climatic context sensitive to the westerlies and also to the shift of the oceanic polar front (Brunetti et al., 2009; Isotta et al., 2014; Crespi et al., 2018).

In this paper, we provide an improvement to the knowledge of the Lateglacial-Holocene transition pattern in the Alps by: i) reconstructing the condition of past glaciers and their evolution in the Gran Paradiso Group, ii) providing a chronological constraint of the last Lateglacial advance by means of the first ^{10}Be ages for the area, and iii) inferring basic information on paleoclimatic conditions based on ELA reconstructions and their variations (ΔELAs).

2. Study area

The area of our study is located in the Gran Paradiso Group (Graian Alps) between 45° 25' - 45° 39′ N and 7° 02' - 7° 28' E, in the sector of the "North-Western Italian Alps" (Fig. 1), according to the International Standardized Mountain Subdivision of the Alps (ISMSA-SOIUSA; Marazzi, 2005). The Gran Paradiso Group culminates at 4061 m with its homonymous peak and hosts the first national park established in the Italian territory (Gran Paradiso National Park, which extends more than 700 km^2). The Gran Paradiso Group represents a key site for the exceptional natural heritage preserved, for the good state of conservation of the ecosystems, and for the reduced anthropic impact affecting the area. The territory ranges from the Aosta Valley in the northern sector to the upper portion of the Orco basin at the southern margin, embracing Rhêmes, Valsavarenche, Valnontey, Valeille valleys, from west to east (Figs. 1 and 2).

The Gran Paradiso Group is one of the internal crystalline massifs outcropping in the axial belt of the Western Italian Alps (Pennidic Domain). It corresponds to a large tectonic window overthrust and surrounded by oceanic and ophiolite units derived from the Piemonte-Liguria ocean (Le Bayon and Ballèvre, 2006; Dal Piaz et al., 2008; Beltrando et al., 2010; Polino et al., 2015). The crystalline rocks of the Gran Paradiso comprise augen gneiss (*Gneiss occhiadini*) and meta-granites originating from porphyritic granitoids (Permian) intruded into a polymetamorphic unit (fine-grained gneiss, paragneiss and micaschists). This derives from Variscan metasedimentary rocks reworked during the Alpine orogeny. Oceanic and ophiolite Mesozoic units consist of calcschists, micaschists, black phyllite (Cretaceous), foliated and massive prasinite, meta-basalt, amphibolite (Jurassic) and serpentinite (Elter, 1987; Gasco et al., 2009; Manzotti et al., 2014; Piana et al., 2017).

During the Pleistocene, most of the study area contributed to the valley glacier of the Dora Baltea compound basins, a complex system of confluent glaciers, several tens of kilometres long, extending from the Mt. Bianco Massif, located well inside the Western Alps, to the upper margin of the Po Plain to the south-east (>120 km in distance). This articulated glacial system fed a large piedmont glacier, which built up the Ivrea Morainic Amphitheatre (IMA), one of the widest morainic amphitheatres in Italy (505 km^2), set up after multiple Pleistocene glacial cycles (Gianotti et al., 2008, 2015). The first signals of the Dora Baltea Glacier retreat from the IMA after the Last Glacial Maximum are dated to 23.8 ± 1.7 ka and 20.1 ± 3.0 ka (^{10}Be exposure ages, Gianotti et al., 2008, 2015). Evidences of alpine deglaciation after the Last Glacial Maximum (LGM) and of the oldest Lateglacial re-advance phases are to be found within the Dora Baltea Basin (Gianotti et al., 2008, 2015). It was also possible to document the most recent Lateglacial stages, since they have been well preserved in the upper Valle d'Aosta (Val Veny and Val Ferret, Porter and Orombelli, 1982) and within the confluent valleys dissecting the most prominent mountain groups of this region. The study area retains a well renowned alpine landscape with typical Alpine erosional landforms (U-shaped valleys, glacial cirques, horns, *arêtes,* trimlines, etc.) and well-preserved Lateglacial and Holocene terminal moraines. The latter are mainly represented by extremely well-shaped sharp ridges testifying the most extended Holocene position reached, in the Italian Alps, during the LIA with only few exceptions (Vanuzzo, 2001; Orombelli, 2011; Lucchesi et al., 2019). Gran Paradiso Group is still among the most glacierized massifs in the north-western Italian Alps where 72 glaciers exist in the study area, mostly mountain glaciers, and to a lesser extent valley glaciers, extend for about 37 km^2 altogether (Salvatore et al., 2015).

The climatic conditions are influenced by the geographic location and by the orographic setting: these can lead to the development of microclimate conditions, since high elevations tend to prevent the access of storms coming from the Atlantic and from the Mediterranean areas (Garzena et al., 2015; Poussin et al., 2019). The distribution of mean annual precipitation (1971–2008) highlights drier conditions in the inner-Alpine valleys, particularly evident in the Aosta Valley (Isotta et al., 2014) with respect to the range of about 1500–2700 mm/year recorded for the North-Eastern, North-Western and South-Western Alps (EEA, 2009). In particular, in the Gran Paradiso Group, annual precipitation ranges from about 480 mm at the main valley floor to about 1400 mm at the Valsavarenche and Cogne valleys head (Isotta et al., 2014). Average monthly rainfall shows two maxima in spring/early summer and autumn (110 mm/month and 180 mm/month, from April to June and November, respectively), and two minima from July to August

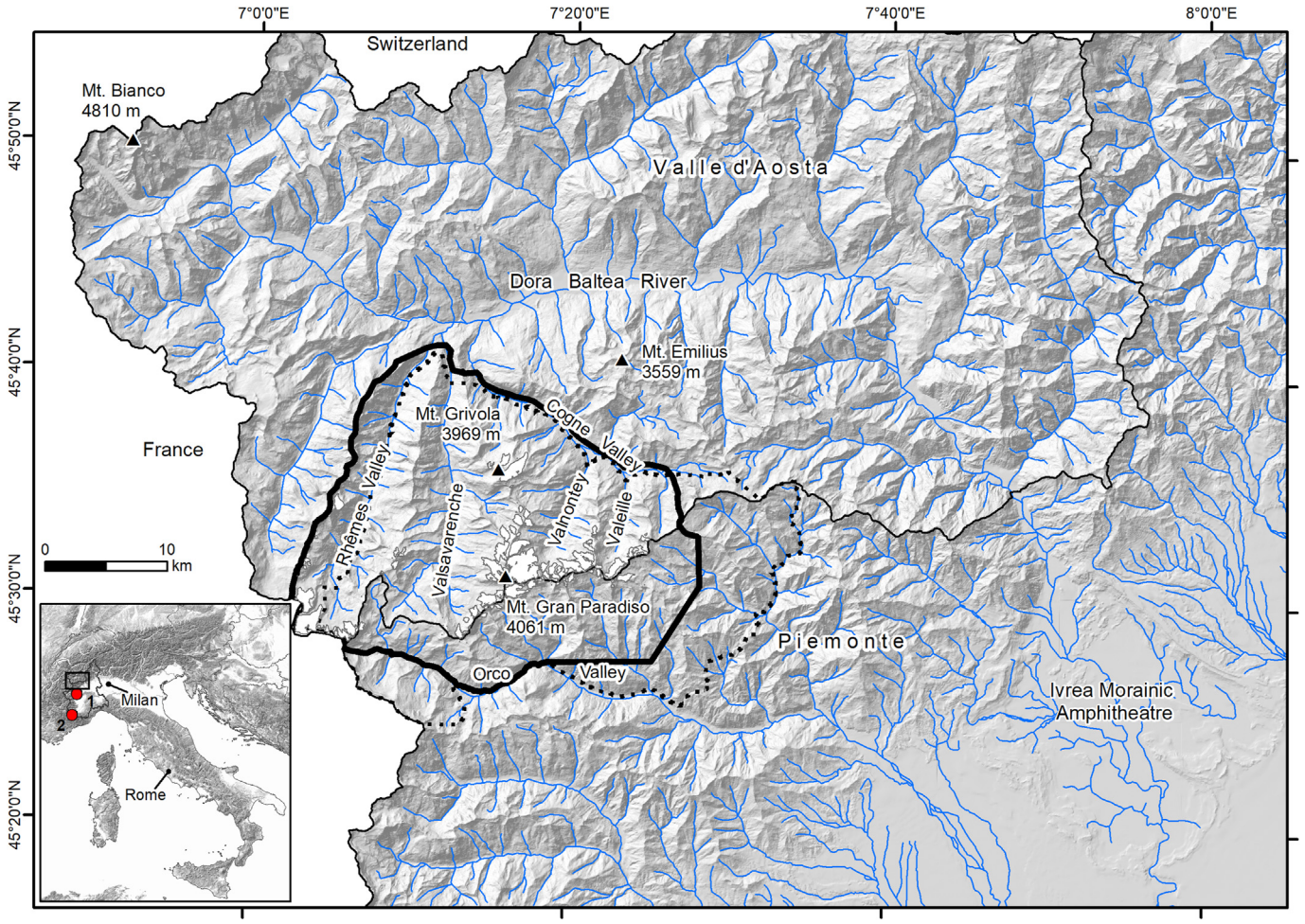

Fig. 1. Location map of the study area (black thick line). The dotted line borders the Gran Paradiso National Park (GPNP); the thin black line indicates the administrative border between the Piemonte and Valle d'Aosta Regions. The basemap is a hillshade in the coordinate system Universal Transverse Mercator, World Geodetic System 1984 datum, Zone 32T (from ISPRA digital elevation models). Circles in the inset (basemap source from https://osm-wms.de/) indicate Lago di Avigliana (1) and Laghi dell'Orgials (2).

and December to March (driest conditions with 71 and 76 mm/month, respectively; Auer et al., 2007; Poussin et al., 2019). On the basis of the HISTALP dataset (Auer et al., 2007) and of the averages over the period 1950–2014, Poussin et al. (2019) calculated average temperature values for the Gran Paradiso National Park of about 9 °C and about −6 °C for the warmest months (JA) and the coldest ones (DJFM), respectively.

3. Material and methods

3.1. Field survey and mapping

Paleo-glacier extent and geometry (Fig. 2) were reconstructed on the basis of photointerpretation, geomorphological and glacial-geological field surveys, cartographic and aerophotographic documents, LiDAR data (from Valle d'Aosta and Piemonte Regions), and historical maps (e.g. Sacco, 1925, 1921a, 1921b; Beschel, 1958). Glacial sediments, glacial drift limits, preserved erosional and depositional landforms provided the baseline data for reconstruction of the individual position reached by the glaciers during the last Lateglacial advance, compared to the maximum extension reached during the LIA (Fig. 2). In particular, the preserved moraines were easily recognized and mapped, and served to delineate the terminal margin of former glaciers (Porter and Orombelli, 1982). The degree of preservation and weathering of landforms and deposits, as well as soil development and thickness, allowed us to distinguish Lateglacial deposits and moraines from those of the LIA, which represent the maximum Holocene extent of local glaciers (GNGFG-CNR, 1986; Vanuzzo, 2001; Orombelli, 2011; Lucchesi et al., 2014). LIA boulders are generally unweathered or poorly weathered, while Lateglacial boulders are more deeply altered and show weathering rinds up to 2 cm in thickness. Boulders made of crystalline rocks pertaining to Lateglacial deposits and moraines show clear differential weathering, resulting in more resistant minerals standing in relief or developing weathering pits in correspondence of less resistant minerals.

The soils on the LIA moraines are 5–20 cm thick and poorly developed (O/A/(B2–B3)/C), while the soil profiles on Lateglacial deposits and moraines are thicker (>30–50 cm) and show a clearer profile differentiation (O/A(E)/B2/B3/C). These features are also documented in many other mountain groups of the Valle d'Aosta and of the Italian Alps (Porter and Orombelli, 1982; Baroni and Carton, 1990, 1996; Carturan et al., 2014; Baroni et al., 2017).

The limit of past glaciers was interpolated on the basis of size of the accumulation basin, aspect, shape of the valley heads, and slope morphometry in places where the glacial deposits were eroded, remobilized, or covered by landslides (Baroni et al., 2018). Finally, following Kuhlemann et al. (2013), on the slopes with limited or

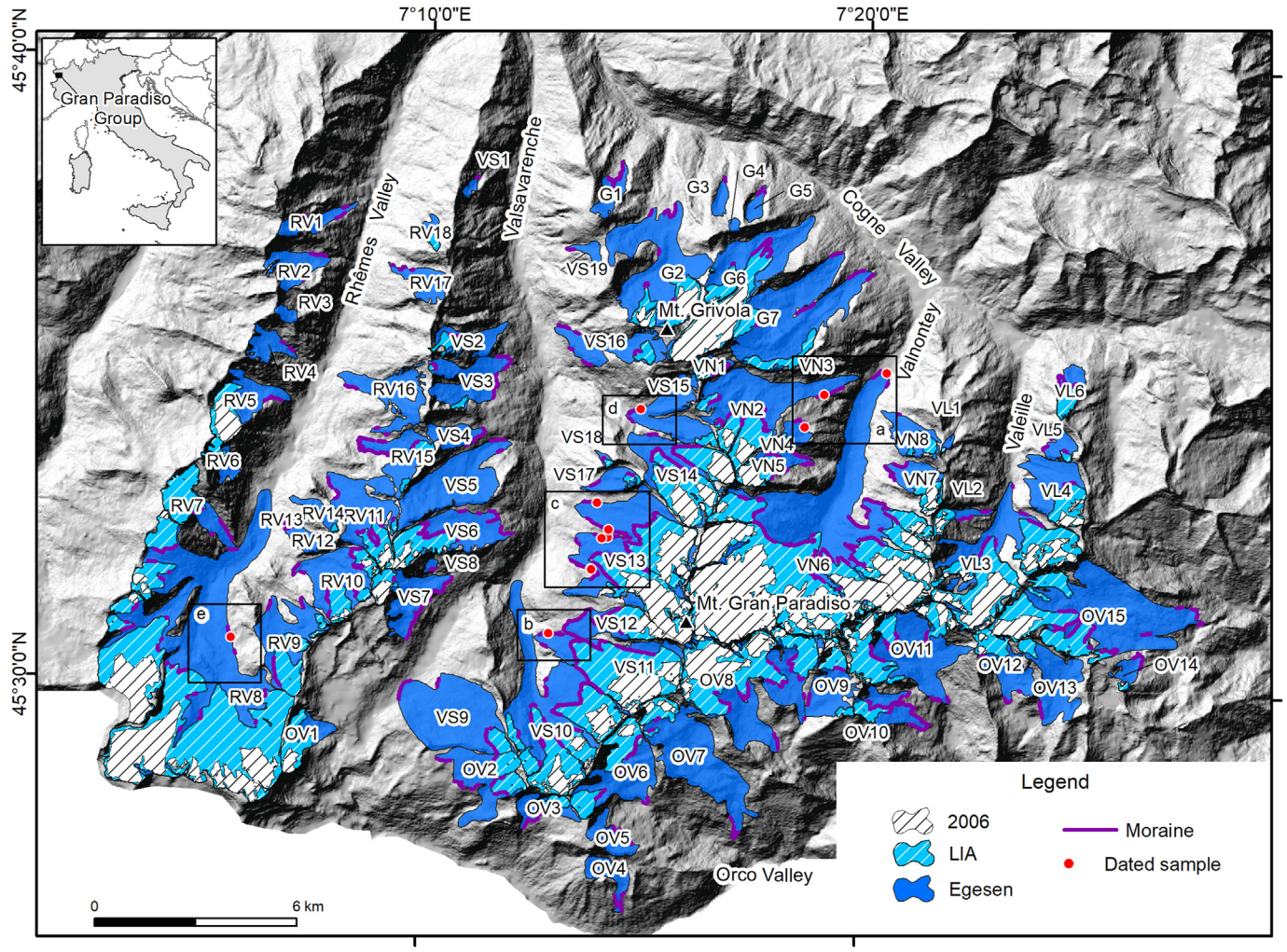

Fig. 2. Distribution of reconstructed paleo-glaciers in the Gran Paradiso Group. Lines in bold represent moraine ridges outlining the reconstructed glaciers. Circles indicate locations of boulders sampled for ^{10}Be exposure dating (see Fig. 3 for details). Individual glaciers were labelled according to the catchment (Supplementary Material, Appendix A, Table A.1).

uncertain evidences, we inferred the extent of past glaciers by comparison with adjacent valleys and adjoining slopes. We estimated any potential uncertainties in limiting glaciers boundaries with mean error value of ±5%, which were even smaller the wider the glacier size.

3.2. Surface exposure dating

Applying a geomorphological and glacial-geological approach and taking into account the geomorphological context, erratic boulders located in key sites were selected for Surface Exposure Dating (SED) using cosmogenic nuclides (^{10}Be) to chronologically constrain the age of the Lateglacial moraines (Figs. 3 and 4; Tables 1 and 2). Erratic boulders were sampled in Valnontey, in Valsavarenche and in the Rhêmes valleys, by adopting well-experienced strategies and criteria which guaranteed reliable ages (Ivy-Ochs et al., 2008; Di Nicola et al., 2009; Baroni et al., 2017, 2018). Best preserved erratic boulders were selected, preferring large and wide-based boulders from the crests of significant moraines located in key sites, while erratic boulders showing evidence of disturbances that derived from gravitational processes, slope instabilities or exhumation were avoided (Baroni et al., 2017, 2018 and references therein). All samples for the application of surface exposure dating were taken from the top-centre portion of stable boulders to reduce shielding and to avoid spallation effects. Topographic shielding factors were determined from the digital elevation model through the GIS model (Codilean, 2006; Li, 2013, 2018) using the Li (2018) ArcGIS toolbox.

Samples for ^{10}Be measurements were prepared at the Earth Science Department (DST) of the University of Pisa (DST-UNIPI) and at the Laboratory of Ion Beam Physics (LIP, ETH Zurich) according to international standards (Kohl and Nishiizumi, 1992; Ivy-Ochs et al., 2006; Ivy-Ochs and Kober, 2008; Wirsig et al., 2016). Sample preparation and analysis for ^{10}Be measurements were performed using quartz as the target mineral (Kohl and Nishiizumi, 1992) extracted from erratics of crystalline rocks (mainly gneiss and schists, Table 1). Beryllium was isolated by using anion and cation exchange columns and selective pH-precipitation. At the end of the treatments, ^{10}Be/^{9}Be ratios of all processed samples were measured at the Laboratory of Ion Beam Physics (ETH, Zurich) using the 600 kV TANDY Accelerator Mass Spectrometry system (Christl et al., 2013). The measured ratios were normalized to the ETH Zurich in house standard S2007N and S2010 with nominal ^{10}Be/^{9}Be ratios of 28.1×10^{-12} and 3.3×10^{-12}, respectively. Both standards have been calibrated relative to ICN 01-5-1 with a nominal ratio of ^{10}Be/^{9}Be $= 2.709 \times 10^{-11}$ (Nishiizumi et al., 2007), which is

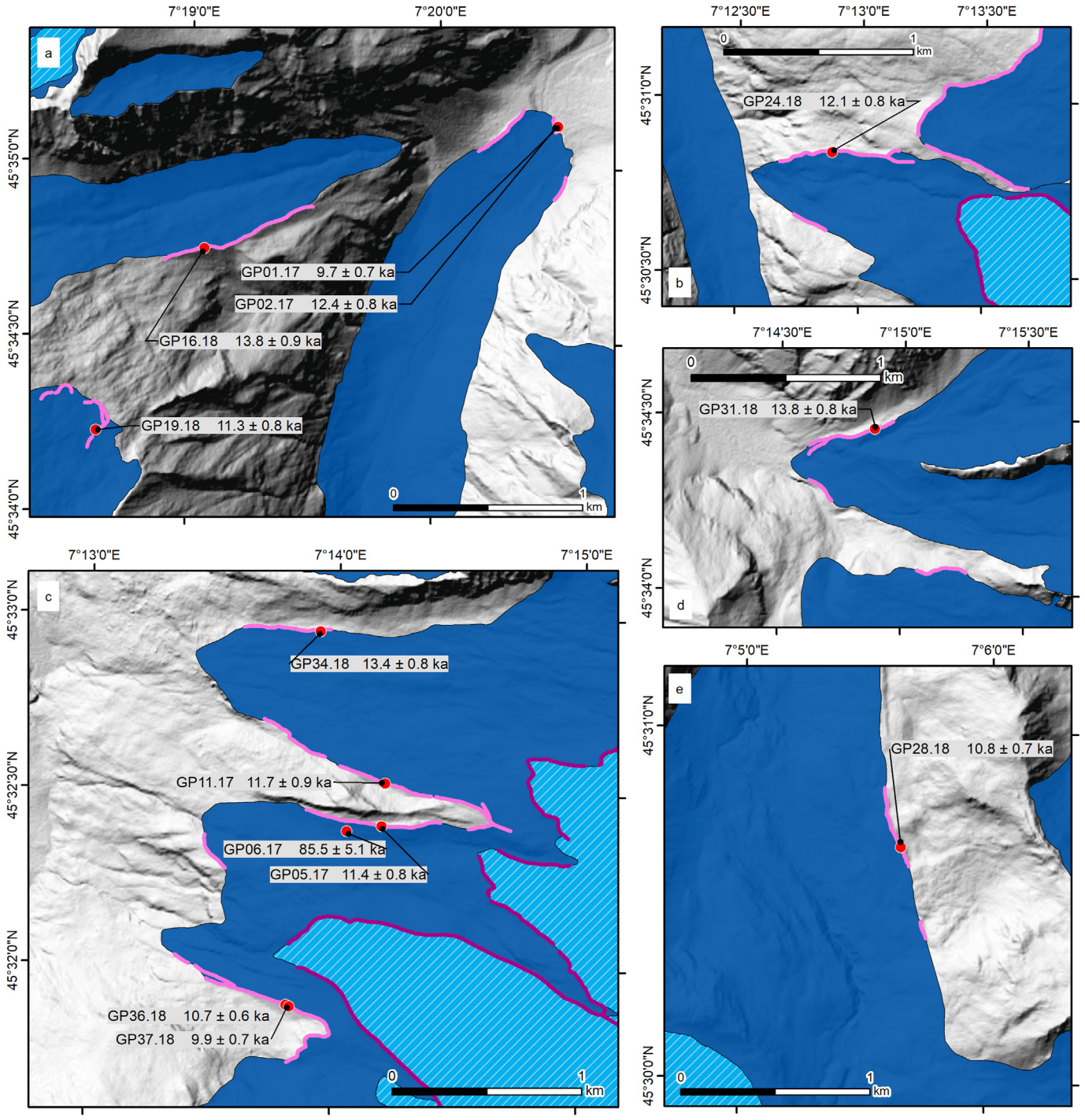

Fig. 3. Enlargements depicting the key sampled sites and the ^{10}Be exposure ages obtained (ka; see Tables 1 and 2 for sample descriptions and ages). Lines in bold represent moraine ridges (Lateglacial and Holocenic moraines are displayed in pink and purple, respectively). (For interpretation of the references to colour in this figure legend, the reader is referred to the Web version of this article.)

associated with a ^{10}Be half-life of 1.387 ± 0.012 Ma (Chmeleff et al., 2010; Korschinek et al., 2010). To calculate ^{10}Be exposure ages we used the "Cronus-Earth" online calculator (Balco et al., 2008; https://hess.ess.washington.edu/math/al_be_v22/alt_cal/Balco_NENA_age_input.html), version 2.2 with a spallation production rate at sea-level and high latitude of 3.93 ± 0.19 ^{10}Be atom g^{-1}_{quartz} a^{-1} 'NENA' (Balco et al., 2009) with an "Lm" time-dependent scaling scheme (Balco et al., 2008). For all the processed samples, a rock density value of 2.65 g cm^{-3} was considered. We applied a conservative surface erosion rate of 1 mm ka^{-1} but made no correction for snow cover, since selected boulders are located in dominant positions with respect to the surroundings, although snow shielding is possibly a source of uncertainty in conditioning exposure ages.

3.3. Paleo-glacier reconstruction

Former glacier outlines (last Lateglacial phase and LIA) were

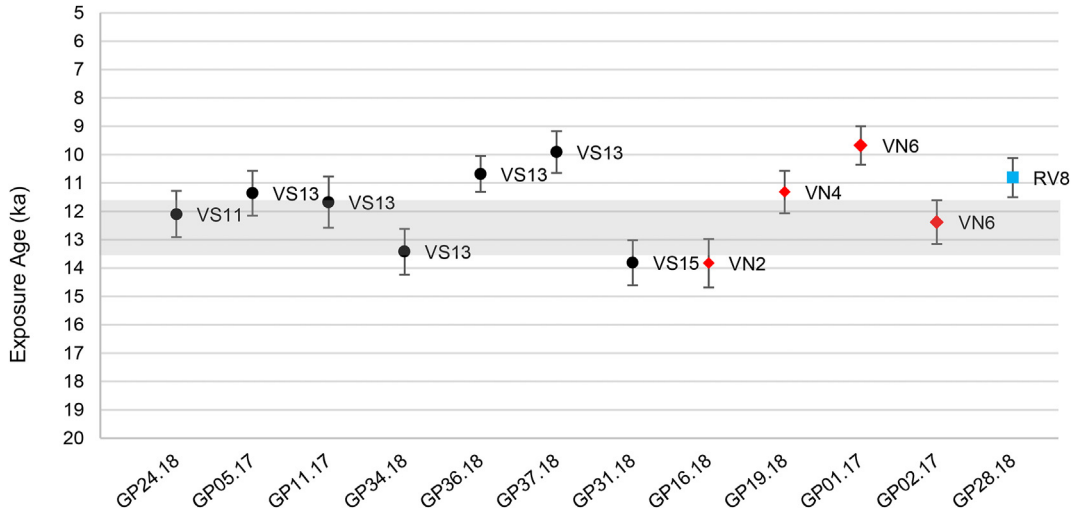

Fig. 4. Plot of the exposure ages obtained for the Gran Paradiso Group with the relative error bars; the time range of the Younger Dryas is evidenced in grey. Black circles, red diamond and blue square indicate samples from Valsavarenche, Valnontey, and the Rhêmes Valley respectively. The labels refer to glacier codes (see Fig. 2 and Supplementary Material, Appendix A, Table A.1). (For interpretation of the references to colour in this figure legend, the reader is referred to the Web version of this article.)

Table 1
List of dated samples. See Fig. 3 for location.

Sample	Valley	Latitude (°N)	Longitude (°E)	Elevation	Boulder size	Lithology	Average sample thickness
ID		WGS 84 (DD)		(m a.s.l.)	(m)		(cm)
GP01.17	Valnontey	45.585	7.341	1685	1.6 × 1.2 × 1.3	Metagranites	1.5
GP02.17	Valnontey	45.585	7.341	1685	3.0 × 2.2 × 1.4	Gneiss	2
GP16.18	Valnontey	45.579	7.317	2350	2.3 × 1.4 × 0.9	Quartz-Schist	1.5
GP19.18	Valnontey	45.570	7.310	2659	2.5 × 1.6 × 0.7	Garnet-bearing Qz-Schist	1.8
GP28.18	Rhêmes	45.511	7.094	2522	1.6 × 1.2 × 0.4	Schist	1
GP05.17	Valsavarenche	45.540	7.236	2666	2.6 × 2.1 × 1.3	Mylonitic metagranite	2
GP06.17	Valsavarenche	45.539	7.234	2588	6.0 × 3.8 × 2.5	Augen Gneiss	1.5
GP11.17	Valsavarenche	45.542	7.236	2640	3.7 × 1.8 × 2.1	Paragneiss	1
GP24.18	Valsavarenche	45.514	7.214	2367	2.4 × 2.3 × 1	Paragneiss	1
GP31.18	Valsavarenche	45.574	7.248	2618	4.8 × 4.2 × 4.7	Gneiss	2.5
GP34.18	Valsavarenche	45.549	7.232	2500	1.8 × 1.2 × 0.9	Gneiss	2
GP36.18	Valsavarenche	45.531	7.230	2549	1.7 × 1.4 × 0.8	Gneiss	1.5
GP37.18	Valsavarenche	45.531	7.230	2543	2.1 × 1.9 × 1.0	Gneiss	1

Table 2
Cosmogenic nuclide data and relative exposure ages of the processed samples. Exposure ages and external uncertainties are reported according to the time-dependent scaling scheme ('Lm') in Balco et al. (2008). External errors (1σ) consider internal uncertainties related to AMS measurement processing, together with the variability of the considered production rate. A reference production rate of 3.87 ± 0.19 at*g-1*yr-1 taken at sea-level and high latitude (SLHL) was applied, based on the North-eastern North America ("NENA") calibration data.

Sample	^{10}Be concentration	Topographic shielding factor	^{10}Be exposure age	^{10}Be age exposure age e = 1mm/ka
ID	(10^5 atoms/g)		(yr)	(yr)
GP01.17	1.413 ± 0.070	0.932	9600 ± 670 (480)	9670 ± 650 (490)
GP02.17	1.796 ± 0.068	0.934	12,250 ± 750 (470)	12,380 ± 770 (480)
GP16.18	3.340 ± 0.124	0.967	13,680 ± 840 (520)	13,830 ± 860 (530)
GP19.18	3.399 ± 0.150	0.980	11,210 ± 740 (500)	11,320 ± 750 (510)
GP28.18	3.011 ± 0.121	0.988	10,710 ± 680 (440)	10,810 ± 690 (450)
GP05.17	3.407 ± 0.168	0.976	11,250 ± 780 (560)	11,360 ± 800 (570)
GP06.17	22.783 ± 0.557	0.948	79,710 ± 4410 (2080)	85,500 ± 5090 (2420)
GP11.17	3.450 ± 0.207	0.971	11,560 ± 890 (700)	11,670 ± 910 (720)
GP24.18	2.999 ± 0.136	0.977	11,980 ± 800 (550)	12,100 ± 810 (560)
GP31.18	3.905 ± 0.117	0.955	13,660 ± 780 (420)	13,810 ± 800 (430)
GP34.18	3.506 ± 0.120	0.950	13,270 ± 790 (460)	13,420 ± 810 (470)
GP36.18	2.969 ± 0.097	0.972	10,590 ± 620 (350)	10,680 ± 630 (360)
GP37.18	2.779 ± 0.154	0.980	9820 ± 720 (550)	9910 ± 740 (560)

manually digitized using on-screen techniques in GIS environment (ArcGIS, ESRI licence and QGis, open source software), and polygons were created in the vector domain (coordinate system: UTM-WGS84, Universal Transverse Mercator-World Geodetic System, 1984 datum, zone 32N). For each shapefile, the associated attribute tables were compiled as exit glacier database, following the World Glacier Monitoring Service (WGMS) guidelines for the compilation of glacier inventory data (Paul et al., 2009, 2010). These were also adopted for the Italian glaciers (Salvatore et al., 2015), and for the reconstruction of past glaciers at regional scale (e.g. Baroni et al.,

2018). For each glacier, attribute tables contain identification information (glacier name and code), latitude and longitude of the glacier centroid, and main glaciological morphometric parameters (area, maximum length, slope, maximum and minimum elevations, mean aspect). A synthesis of glaciological parameters and quantitative data of the reconstructed former glaciers is supplied in the supplementary material (Appendix A, Table A.1).

Following Porter (1975) and Porter and Orombelli (1982), paleo-glacier surface topographies were depicted drawing vector contour lines with a convex and a concave shape in the ablation and accumulation areas of glaciers, respectively, considering 50 m of equidistance for each reconstructed phase (last Lateglacial readvance, this paper; and LIA, Gennaro, 2020). The reconstructed contours were linked to the vector contour lines of present-day ice-free areas, extracted from the LiDAR data for the Valle d'Aosta Region sector combined with the vector contour lines of the Piemonte Region. The ice-free area resulted unchanged over the whole time-range. DEMs were processed using ArcGIS (ESRI software, 3D Analyst license) by creating a TIN (Triangular Irregular Network) surface model from the reconstructed contour lines, applying a Delaunay conforming triangulation. DEMs with a cell size of 10 × 10 m were obtained using a conversion tool from tin to grid raster surfaces.

3.4. ELA and paleoclimate parameter reconstruction

ELA values were obtained by applying both Accumulation Area Ratio (AAR) and Area-Altitude Balance Ratio (AABR) methods. The AABR method takes into account the glacier hypsometry and the mass balance gradient, certainly more reliable than the AAR method for reconstructing the paleo-glacier ELAs (Osmaston, 2005; Rea, 2009), although some uncertainty in the calculated results is linked to the balance ratio adopted. Furthermore, since the AAR method has often been used since the 1970s for reconstructing the ELAs of paleo-glaciers, we applied both methods for comparison with those of previous authors and of other Alpine mountain groups. Following earlier works conducted in the Italian Alps and in the Northern Apennines (e.g. Gross et al., 1977; Baroni et al., 2017, 2018), ELAs were calculated adopting an AAR of 0.67 ± 0.05 for valley glaciers and of 0.50 ± 0.05 for cirque glaciers (Porter, 1975); as regards the AABR, the Balance Ratio adopted was 1.59 with errors of ±0.6 (Rea, 2009; Baroni et al., 2018). Although the ELAs of glaciers in 2006 CE certainly represent an "environmental ELA" *sensu* Anderson et al. (2018), we also calculated the ELA for existing glaciers in the study area, since it is an excellent proxy for climate variability and for representing the currently lowest boundary of climatic glacierization in the Gran Paradiso Group (Zemp et al., 2007; Rea et al., 2020).

Hypsometry and ELA calculation were obtained with a Python scripted ArcGIS Tool by following the method adopted by Pellitero et al. (2015) to calculate the AAR-ELAs and AABR-ELAs automatically (see Supplementary Material, Appendix A, ELA Toolbox). For each time-step, our tool script allows to keep all the glacier features in a single shapefile, discerning them by means of an alphanumeric primary key. In our particular case, the glacier code was used as primary key in the shapefile.

Lateglacial and LIA ELAs (m a.s.l.) allowed us to calculate the delta-ELAs (ΔELAs, m) to reconstruct precipitation and past temperatures (Tables 3 and 4). Temperature variations (ΔT, °C) were calculated assuming precipitation amounts close to present-day precipitations and applying a standard average lapse rate of 0.65 °C/100 m. We also provided ΔTs that were obtained by applying standard average lapse rates of 0.6–0.8 °C/100 m (Braithwaite and Zhang, 2000). Moreover, we calculated ΔT by considering the sensitivity of ELA to the summer temperatures of 115 m $°C^{-1}$ (0.87 °C/100 m), which was considered for glaciers hosted in the French Alps (Rabatel et al., 2013; Protin et al., 2019). This lapse rate was however excluded because it provides negative precipitation values at the reconstructed Lateglacial ELAs (see below).

Paleo-temperatures (°C) of the hottest (July) and coldest (January) months were inferred from independent proxies such as Chironomids and pollen associations (Walker et al., 1997; Walker and Cwynar, 2006; Larocque and Finsinger, 2008; Ortu et al., 2008; Heiri et al., 2011, 2014b; Brooks and Heiri, 2013; Spagnolo and Ribolini, 2019). We selected two sites to extrapolate the temperatures of the hottest and coldest months at the Egesen ELAs that are not located in the Gran Paradiso Group, but are the closest to the study area currently available. In particular, we used Chironomid assemblages at the Lago Piccolo di Avigliana, (365 m a.s.l.; 45° 3′ N, 7° 23′ E, about 50 km to the south with respect to the Gran Paradiso), where Larocque and Finsinger (2008) reconstructed the YD T_{jul} of about 16.0 °C. The YD T_{jul} was adjusted to the Egesen ELAs (m a.s.l.) by applying standard average lapse rates of 0.65 °C/100 m (standard average lapse rates ranging from 0.6 to 0.8 °C/100 m were also applied, Table 4). We adjusted the coldest month temperature obtained from pollen associations found at the Laghi dell'Orgials (at 2240 m a.s.l.; 44° 12′ N, 7° 9′ E; about 145 km to the south with respect to the Gran Paradiso; Ortu et al., 2008) to the elevations of the Egesen ELAs (m a.s.l.), by applying the same standard lapse rate. The maximum and minimum temperatures of the hottest and coldest YD months at the Egesen ELAs were used to infer daily T at the ELAs and the YD summer temperatures, assuming that yearly temperature trends can be approximated by a sine function. We compared our results also to other Alpine sites for chironomid-based temperature reconstruction (Heiri et al., 2011, 2014b).

Considering the YD summer temperatures at the Egesen ELAs, we inferred paleo-precipitations during the YD by application of precipitation/temperature (P/T) equations (Ohmura and Boettcher, 2018):

$$1)\ P_{ann} = 5.87\,T^2 + 230T + 966\ \left(\text{quadratic approximation}\right)$$

$$2)\ P_{ann} = 264.1\,T + 957\ (\text{linear approximation}),$$

where P_{ann} and T are the annual precipitation amount (mm) and the summer temperature (°C), respectively.

3.5. Glacier volumetric variation

Glacier volumetric variations were obtained by comparing digital elevation models related to different time-steps considered here (last Lateglacial phase, LIA, and 2006 CE) by using DEMs already available (2006) and derived from reconstructed paleo-topographies. DEMs in grid format were re-sampled to a common cell size of 10 × 10 m.

The volume (ΔV) in the time interval (hereafter identified as t_1 and t_2) was obtained through the relation:

$$\Delta V = \Delta z \times A_{max},$$

with A_{max} representing the largest area between t_1 and t_2, and Δz representing the average elevation change between the DTMs of the considered time interval over the A_{max} area (Fischer, 2011; Carturan et al., 2013a, 2013b; Fischer et al., 2015). The average mass balance (M) was calculated as:

Table 3
Summary of mean ELA values in m a.s.l. (a), average ELAs weighted on the glacier extension (b), and ΔELAs (m) of the weighted mean values (c), obtained using AAR e AABR methods for the entire Gran Paradiso Group and distinguished for different valley/sectors (see Supplementary Materials, Appendix A Table A.3 for a detailed list of glaciers considered).

	Area (km^2)			Methods	a) Mean ELAs (m a.s.l.)			b) Weighted mean ELAs (m a.s.l.)			c) ΔELA (m)		
	Egesen	LIA	2006		Egesen	LIA	2006	Egesen	LIA	2006	LIA-Egesen	2006-Egesen	2006-LIA
Gran Paradiso Group	239	104	37	AAR	2718 ± 32	2998 ± 19	3169 ± 13	2764 ± 32	2995 ± 19	3157 ± 13	231 ± 13	394 ± 19	163 ± 6
				AABR	2755 ± 36	3017 ± 21	3164 ± 14	2820 ± 36	3036 ± 21	3163 ± 14	216 ± 14	342 ± 22	126 ± 7
Rhêmes Valley	55	25	7	AAR	2608 ± 36	2983 ± 16	3069 ± 11	2723 ± 36	2915 ± 16	3033 ± 11	192 ± 20	310 ± 25	117 ± 5
				AABR	2656 ± 37	2991 ± 18	3057 ± 13	2758 ± 37	2957 ± 18	3014 ± 13	199 ± 20	256 ± 25	57 ± 5
Valsavarenche	59	24	8	AAR	2776 ± 31	3029 ± 18	3194 ± 15	2815 ± 31	3026 ± 18	3190 ± 15	211 ± 13	376 ± 16	164 ± 3
				AABR	2820 ± 36	3050 ± 23	3199 ± 17	2874 ± 36	3069 ± 23	3207 ± 17	195 ± 13	334 ± 19	138 ± 6
Valnontey	40	24	12	AAR	2878 ± 31	3020 ± 26	3175 ± 17	2791 ± 31	3011 ± 26	3208 ± 17	220 ± 5	416 ± 14	196 ± 9
				AABR	2898 ± 35	3061 ± 26	3171 ± 18	2868 ± 35	3087 ± 26	3224 ± 18	219 ± 9	356 ± 17	137 ± 8
Grivola	22	6	3	AAR	2517 ± 38	3109 ± 23	3273 ± 17	2631 ± 38	3144 ± 23	3258 ± 17	513 ± 15	627 ± 21	114 ± 6
				AABR	2556 ± 43	3107 ± 30	3267 ± 20	2731 ± 43	3123 ± 30	3270 ± 20	392 ± 13	539 ± 23	147 ± 10
Valeille	13	7	2	AAR	2732 ± 30	2860 ± 16	2983 ± 16	2720 ± 30	2862 ± 16	2925 ± 16	142 ± 14	205 ± 14	63 ± 0
				AABR	2747 ± 31	2876 ± 20	2992 ± 15	2750 ± 31	2881 ± 20	2936 ± 15	131 ± 11	186 ± 16	55 ± 5
Orco Valley	51	18	4	AAR	2781 ± 27	2987 ± 17	3260 ± 8	2794 ± 27	3042 ± 17	3218 ± 8	248 ± 11	424 ± 19	176 ± 8
				AABR	2815 ± 32	3005 ± 18	3250 ± 9	2845 ± 32	3069 ± 18	3204 ± 9	224 ± 14	359 ± 23	135 ± 9

Table 4
Reconstructed temperature and precipitation at the ELAs (calculated with AAR and AABR methods) of the Egesen glaciers during the YD cold period. Lapse rates from Zemp et al. (2007) refer to the hottest (*) and the coldest (**) months.

Lapse rate		ΔT (°C) LIA-YD	ΔT (°C) 2006-YD	ΔT (°C) 2006-LIA	Hottest month temperature	Coldest month temperature	P (annual) (quadratic approximation)	P (annual) (linear approximation)
Reference	°C/100 m	°C	°C	°C	°C	°C	mm	mm
Zemp et al. (2007)	0.71* 0.54**	–	–	–	−1.03/−1.43	−18.83/−19.13	540/460	442/338
Braithwaite and Zhang (2000)	0.60	1.39/1.30	2.36/2.06	0.97/0.76	1.61/1.27	−19.14/−19.48	1091/1012	1099/1010
Braithwaite and Zhang (2000)	0.65	1.50/1.40	2.56/2.23	1.05/0.83	0.41/0.04	−19.41/−19.77	827/746	795/698
Heiri et al. (2011, 2014b)	0.67	1.55/1.45	2.63/2.30	1.09/0.85	−0.07/−0.45	−19.51/−19.89	725/645	673/574
Braithwaite and Zhang (2000)	0.70	1.62/1.51	2.75/2.40	1.13/0.89	−0.79/−1.19	−19.67/−20.06	578/497	491/387
Braithwaite and Zhang (2000)	0.80	1.85/1.73	3.14/2.74	1.3/1.02	−3.19/−3.64	−20.19/−20.64	127/47	–

$$M = \left((\Delta V \times \rho) \overline{A}^{-1} \right) \Delta t^{-1},$$

where ρ is the glacier mean density, A is the mean area between t_1 and t_2, and Δt is the time interval (in years) between the two periods (Carturan et al., 2013b). To obtain the geodetic mass budget rate (m w.e. yr^{-1}), the mean density of ice was assumed to be equal to 850 ± 60 kg/m^3 (Huss, 2013).

The results obtained were discussed taking into account the key time-steps considered (YD, LIA, 2006), and they furnished new paleoclimatic data to characterize the YD in the Western Alps.

4. Results

A complex and articulated system of moraines and glacial deposits outcropping outside the limit of LIA moraines document the pre-LIA glacial phase occurred in the Gran Paradiso Group. The 73 reconstructed glaciers covered a total area of about 240 km^2 (Figs. 2 and 3), retaining an estimated ice volume exceeding ~17.5 km^3 (this minimum volume was calculated without considering the ice stored in the glaciers existing at 2006 CE). Ice bodies occupied large portions of the tributary valleys of the Gran Paradiso Group, covering not only the valley heads but also extending to the ridges between the valleys. In the entire massif we identified 17 compound basin(s) valley glaciers, 27 simple basin valley glaciers, 7 miscellaneous valley glaciers, and 22 mountain glaciers. Detailed information for each reconstructed glacier in the Gran Paradiso Group is provided in the Supplementary Material (Appendix A, Table A.1).

Considering all the reconstructed glaciers for the last Lateglacial advance, we distinguished seven size-classes of glaciers following the WGMS recommendations for present glacier inventories (Paul et al., 2009, 2010; Gardent et al., 2014; Salvatore et al., 2015).

This study was also useful to supply quantitative information on reconstructed paleo-glaciers at a regional scale (e.g. Baroni et al., 2018, Fig. 5). Paleo-glaciers with an area >1 km^2 (~60% of the total number) covered about 94% of the total glacierized area. About 16 glacial bodies exceeding 5 km^2 (~22% of the total number of glacial bodies) covered ~65% of the total area (with ~34% of the total surface represented by the size class 5–10 km^2). Four glaciers only, embracing ~33% of the total glacierized area, extended for more than 10 km^2 each, and they reached minimum elevations ranging from 1700 to 2300 m a.s.l. with their front. The head of the Rhêmes Valley and of Valnontey hosted the two widest glaciers, which retained ~24% of the total glacierized area in this massif, covering 29.2 and 28.2 km^2, respectively (Fig. 2; Supplementary Material, Appendix A, Table A.1).

About 25% of the reconstructed glaciers was comprised in the size class 2–5 km^2 and more than 23% in the size class 0.5–1 km^2,

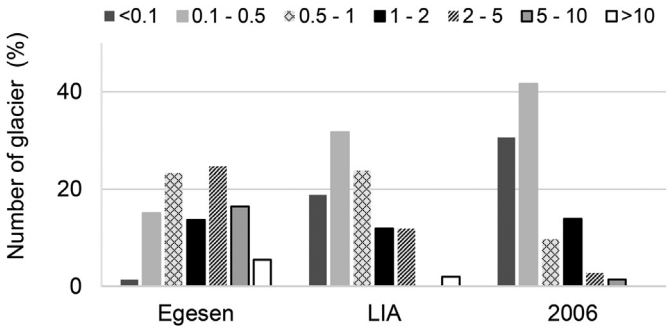

Fig. 5. Distribution of the Gran Paradiso Group glaciers during the Egesen, the LIA and in 2006 CE, according to different size classes (km^2, following Paul et al., 2010, 2009) based on the total number of glaciers (%). 2006 CE data from Salvatore et al. (2015).

which covered ~50 km^2 and ~13 km^2 (corresponding to ~21% and over ~5% of the total glaciated area, respectively).

Finally, the size classes 1–2 km^2, 0.1–0.5 km^2 and <0.1 km^2 covered ~7% of the total area corresponding to ~14%, ~15% and ~1% of the total number of glaciers, respectively (Figs. 2 and 5; Supplementary Material, Appendix A, Table A.1).

Considering the orographic setting of the study area and the prevailing S–N orientation of the main valleys, the distribution of the glaciers was not uniform and most of the glaciers faced towards the northern sectors both in terms of number and areal extension, with the only exception of the Orco Valley glaciers with a prevailing SE aspect (Supplementary Material, Appendix A, Fig. A.1). More than 50% of the glacial bodies developed on north-facing slopes, embracing ca. 63% of the total glacierized area, whereas only about 17% of the glaciated area developed on south-facing slopes, mostly in the Orco Valley (Fig. 2). Different aspects, together with glacier size (i.e. extent of the accumulation basin) also conditioned the minimum elevation reached by paleo-glacier fronts, with an average of 2235 m (Supplementary Material, Appendix A, Fig. A.2). Table A.2 and Fig. A.3 show glacier distribution in different basins and sectors, each distinguished by class size.

Selected erratic boulders located on top of well-preserved moraines and sampled at key sites supplied the first ^{10}Be exposure ages available for the study area, which allowed to chronologically constrain the pre-LIA glacial advance stadial (Tables 1 and 2; Figs. 3 and 4). This glacier advance is well documented by moraines and glacial deposits outcropping outside the limit reached by the glaciers during the LIA, which represented the maximum Holocene position (Vanuzzo, 2001; Lucchesi et al., 2019).

In Valnontey, the frontal margin of the widest Lateglacial glacier is well outlined by lateral moraines deposited in proximity of the homonymous village at about 1680 m a.s.l. (Figs. 2 and 3). Erratic boulders, located on the right lateral-frontal moraine, indicate that the main glacier of Valnontey reached this position before 12.4 ± 0.8 ka (and 9.7 ± 0.7 ka; samples GP02.17 and GP01.17, respectively; Fig. 3a). We consider the younger date to be "very" minimal and the older one to be closer to the "true" age of the terminal moraine. The second widest glacier hosted in Valnontey occupied the tributary Lauson Valley but did not reach the main tongue of the valley glacier; two Lateglacial right lateral moraines supplied the exposure ages of 13.8 ± 0.9 ka and 11.3 ± 0.8 ka, respectively (GP16.18 and GP19.18; Fig. 3a).

The best-preserved moraines in Valsavarenche lie on the right side of the valley. In particular, the position reached by the Moncorvè Glacier (VS11 in Fig. 3b) is delineated by a right lateral moraine. An erratic boulder situated at about 2365 m a.s.l. yielded an exposure age of 12.1 ± 0.8 ka (GP24.18; Fig. 3b). The wide Lavacciù-Montandeyné Glacier (VS13 in Fig. 3c) was characterized by two main lobes (>10 km^2), as testified by two left and two right lateral moraines. As regards the southern lobe, three samples returned exposure ages of 11.4 ± 0.8 ka, 10.7 ± 0.6 and 9.9 ± 0.7 ka, respectively (GP05.17, GP36.18 and GP37.18; Fig. 3c). Samples collected on the moraines of the northern lobe (GP11.17 and GP34.18) were dated to 11.7 ± 0.9 and 13.4 ± 0.8 ka, respectively (Fig. 3c). One sample (GP06.17) provided an outlier age, much older than expected (85.5 ± 5.1 ka; Fig. 3c). Considering the location of the huge sampled boulder, located well below the LGM erosional trimline, the sampled surface most probably retains the effect of an inherited exposure acquired above the LGM trimline during the Late Pleistocene, before it fell and was transferred onto the Lateglacial moraine that we sampled. The VS15 glacier's Lateglacial left lateral moraine was dated 13.8 ± 0.8 ka (sample GP31.18; Fig. 3d). The reduced Chi-squared statistics (Balco, 2011) of the five samples of the Lavacciù-Montandeyné Glacier led us to consider that the ages we obtained do not depend on internal error but reflect different ages of the collected samples.

Finally, in the Rhêmes Valley, the sample (GP28.18) collected from the right lateral moraine of the widest valley glacier of the massif (~29.2 km^2) yielded a minimum age of 10.8 ± 0.7 ka (Fig. 3e). A very minimum age for this moraine was provided by a paleosol developed on the top and buried by an advancing rock glacier (3965 ± 140 ^{14}C years BP, 4081–4830 cal BP), indicating that the rock glacier had been active at least since the early Late Holocene (Mortara et al., 1992).

Most of the obtained dates overlap, indicating that the terminal moraines dated here developed during a period of glacier advances and/or standstills at the end of the Lateglacial (between ca. 13 and 11 ka).

The reconstructed paleo-topography of the glaciers hosted in the Gran Paradiso Group during the last Lateglacial stadial recorded ELA values ranging from 2180 ±20 m to 3270 -10/+20 m (obtained with the AAR method) and 2160 -20/+30 m to 3300 ± 20 m (obtained with the AABR method; Supplementary Material, Appendix A, Table A.3). The calculated ELA values vary according to several parameters, especially geographic location (different hydrographic basins), glacier extent, slope, hypsometry, and aspect. Considering the reconstructed paleo-glaciers with an area >1 km^2 (n = 44), which covered about 94% of the total glacierized area, ELA values range from 2390 ± 20 to 3060 ± 30 m using the AAR method, while the AABR method returned values comprised between 2440 ± 30 and 3100 ± 45 m (Supplementary Material, Appendix A, Table A.3).

The average ELA weighted on the glacier extension of the last Lateglacial stadial in the Gran Paradiso Group varies from 2764 ± 32 m to 2820 ± 36 m a.s.l. when applying the AAR and the AABR methods, respectively (corresponding to 2718 ± 32 m and 2755 ± 36 m if we consider the mean ELA values; Fig. 6, Table 3; Supplementary Material, Appendix A, Table A.3). Distinguished by different hydrographic basins (and sectors) of the mountain group, the weighted average ELA value ranged from 2631 ± 38 m (AAR) and 2731 ± 43 m (AABR) in the Grivola sector to 2815 ± 31 m (AAR) and 2874 ± 36 m (AABR) in Valsavarenche. ELAs close to the highest value recorded in the study area also characterize the southern sector (Orco basin), where the majority of reconstructed glaciers were facing south (Fig. 6, Table 3; Supplementary Material, Appendix A, Table A.3).

During the LIA, the Gran Paradiso Group hosted 101 glaciers covering more than 104 km^2 and retaining more than 3.5 km^3 of freshwater (Gennaro, 2020). The maximum position of the LIA glaciers is constrained by well-preserved lateral, latero-frontal and frontal moraines characterized by a well-defined sharp topographic profile. The glacial drift of this phase can be distinguished from older deposits (i.e. Lateglacial) considering the weathering degree of boulders and cobbles, soil profile, and thickness. LIA moraines

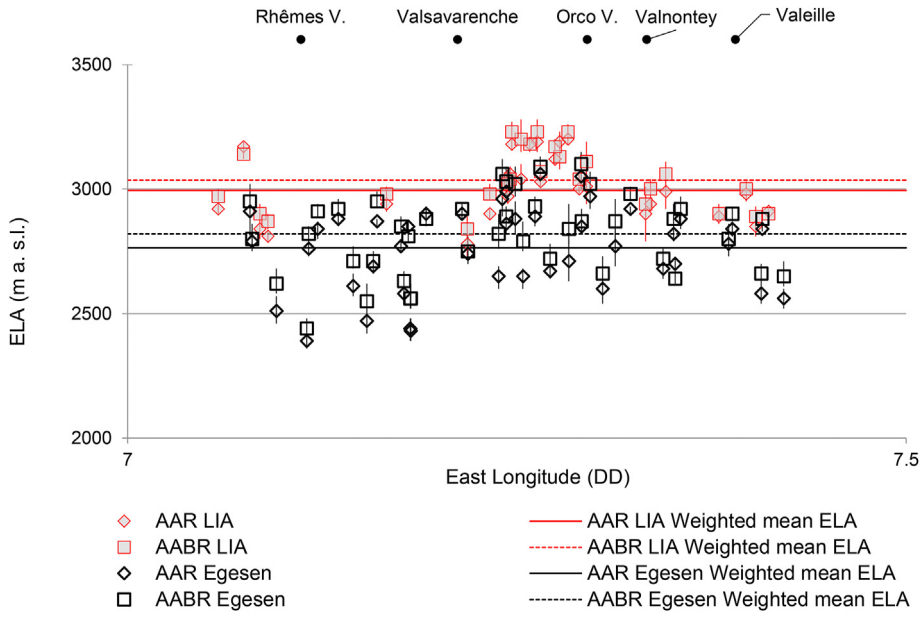

Fig. 6. Equilibrium Line Altitudes (ELA, m a.s.l.) during the Egesen and the LIA, calculated with both AAR and AABR methods, considering glaciers covering an area exceeding 1 km^2. (For interpretation of the references to colour in this figure legend, the reader is referred to the Web version of this article).

are well distributed at the forefield of present glaciers and can be mainly dated back to the last advance phase of the 19th century (Orombelli, 2011; Lucchesi et al., 2014). Compound basin valley glaciers (n = 8; ca. 8% of LIA glaciers) and simple basin valley glaciers (n = 48; ca. 47% of LIA glaciers) covered more than 84 km^2 (ca. 81%) of the total glaciated area (Gennaro, 2020). The remnant 45 mountain glaciers (mainly cirque glaciers, ca. 45% of LIA glaciers) were distributed all over the study area and covered about 20% of the total glacierized area.

Between the Lateglacial stadial dated here and the LIA we observed a ΔELA (using AAR and AABR methods) ranging from 513 ± 15 / 392 ± 13 m in the Grivola area to 142 ± 14 / 131 ± 11 m in the Valeille area. In the entire Gran Paradiso Group the ELA was situated at about 231 ± 13 / 216 ± 14 m lower than during the LIA (weighted mean using AAR and AABR methods, respectively). The ΔELA ranged from 280 ± 13 m to 262 ± 14 if we apply the mean value of Egesen and LIA glaciers, using AAR and AABR methods, respectively (Table 3; Supplementary Material, Appendix A, Table A.3).

The maximum extension reached by the Gran Paradiso glaciers during the last Lateglacial stadial (ca. 240 km^2) and by the LIA (104 km^2) differs in extension by over 56% (about 135 km^2), while the glaciers in 2006 CE covered only 15% of the area glaciated during the last glacial stade before the LIA (see Supplementary Material, Appendix A, Table A.4 for details).

Approximately 26% (n = 19) of the total number of last Lateglacial glaciers did not exist during the LIA maximum advance. Therefore, the increase in terms of number of glaciers between the last Lateglacial phase (n = 73) and the LIA (n = 101) indicates the fragmentation of the widest Lateglacial glaciers into several smaller glacial bodies, that eventually advanced during the LIA. A clear example is given by the widest and longest glacier of Valnontey (VN6, Grand Croux-Tribolazione-Dzasset Glacier, Supplementary Material, Appendix A, Table A.1), covering about 28 km^2 (max length >9 km; minimum elevation: 1700 m).

The different areal extent of glaciers during the last Lateglacial and the LIA was accompanied by a difference in volume of over ca. 13.5 km^3, as indicated by the geodetic mass balance calculated using the digital elevation models (DEMs) reconstructed for the LIA and the last Lateglacial stadial (Fig. 7). According to our reconstruction, LIA glaciers hold about one-fourth of volume compared to the Lateglacial.

The volumetric difference between the last Lateglacial and the LIA was about 11.5 ± 0.8 km^3 w.e., assuming an ice density equal to 850 ± 60 kg/m^3 (Huss, 2013). The glaciers between the LIA and 2006 CE lost about 3.3 ± 0.3 km^3 w.e. (approximately 47 ± 3 m w.e.), with a geodetic mass balance rate of about −0.25 m w.e. yr^{-1} on an averaged area of ca. 70 km^2.

5. Discussion

The ^{10}Be exposure ages presented in this paper allow the timing of the last pre-LIA glacier advance in the Gran Paradiso Group to be dated back to 13–11 ka (Fig. 4). This glacial advance is correlated to the regional Egesen stadial *Auct.*; (13.5 ± 1.1 ka for the Val di Rabbi from Favilli et al., 2009; 13.5–11.5 ka, Ivy-Ochs, 2015; >12.3 ± 0.7–11.2 ± 0.8 for the La Mare and Careser glaciers, Baroni et al., 2017). This Lateglacial advance corresponds to the Younger Dryas stadial in Scandinavia and to the Greenland stadial 1 in the INTIMATE event stratigraphy, the last climatic deterioration that punctuated Termination I (Mayr and Heuberger, 1968; Mangerud et al., 1974; Gross et al., 1977; Furrer et al., 1987; Kerschner et al., 2000; Ivy-Ochs et al., 2008, 2009; Rasmussen et al., 2014; Moran et al., 2016).

Although double-crested and accretion lateral moraines are locally present, documenting successive phases of glacier advance, geomorphological features and glacial deposits show no evidence of a double set of moraines clearly identified for every reconstructed glacier attributed to this phase (Figs. 2 and 3). Cosmogenic nuclide data do not highlight a clear double response of the Gran Paradiso glaciers to the Egesen stadial, unlike other Alpine sites (Maisch, 1982; Furrer et al., 1987; Kerschner, 2009; Ivy-Ochs, 2015; Chenet et al., 2016; Baroni et al., 2017; Federici et al., 2017). Alternative explanations for the age distribution we obtained are i) the presence of stacked lateral moraines formed in minor successive stages of advancement, possibly including the Early Holocene

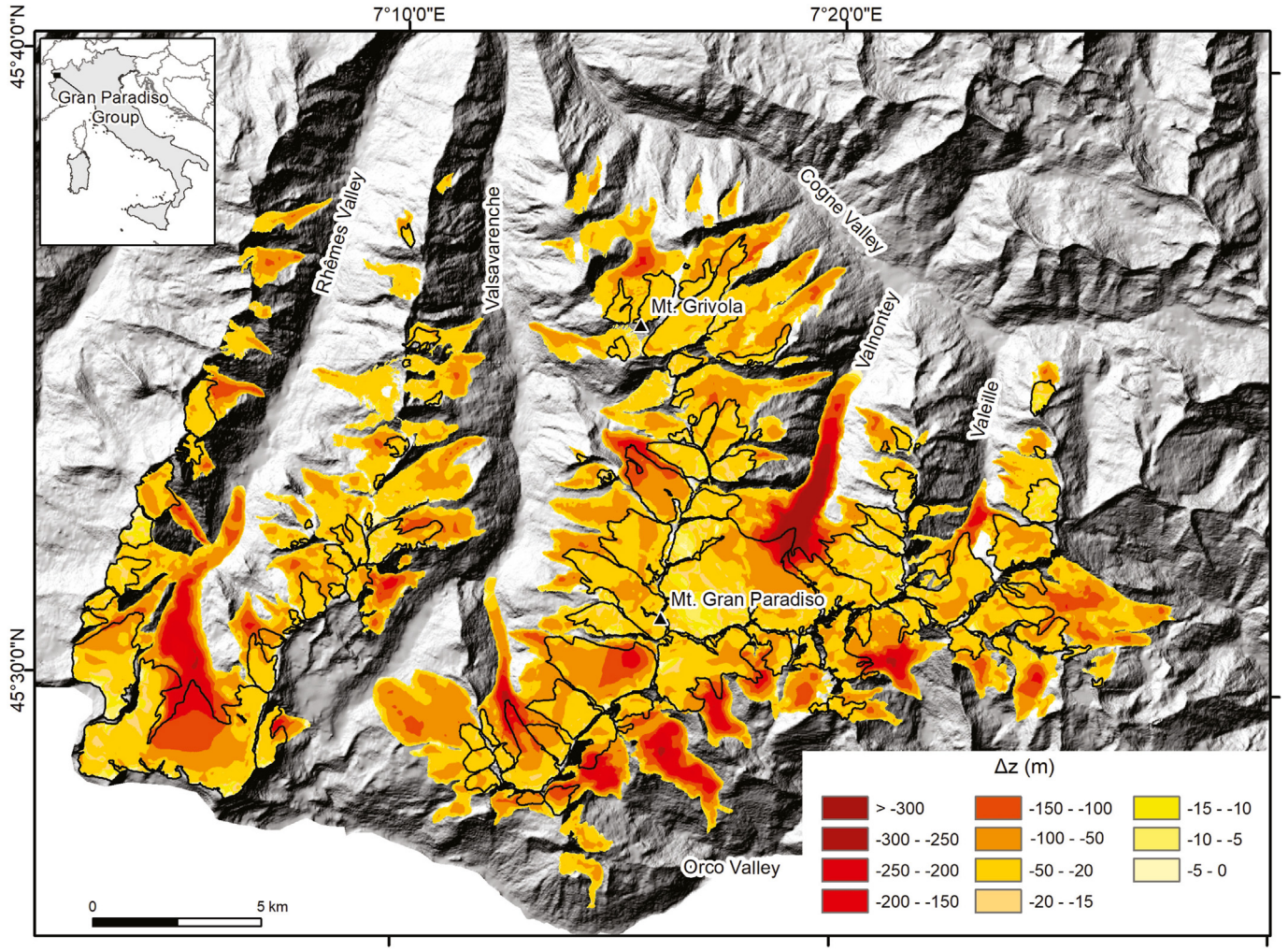

Fig. 7. Difference map between the Egesen and LIA DEMs for the entire glacierized area of the Gran Paradiso Group. The chromatic scale shows the thickness variation classes (Δz, in metres). (For interpretation of the references to colour in this figure legend, the reader is referred to the Web version of this article).

glacier advance, and ii) a diachronic response of paleoglaciers in the Gran Paradiso Group to the YD cold phase. However, even in this case, glacier response(s) to the YD cold period occurred between 11 and 13 ka.

The ELAs we reconstructed for the Egesen stadial and for the LIA are well comparable with some sites in the Alps (e.g. Southern Rhaetian Alps, Baroni et al., 2017, Fig. 8), but are very different from other Alpine localities (e.g. Maritime Alps, Federici et al., 2017; Krnica Valley, Kozamernik et al., 2018). The ELA position in the Alps during the Egesen shows an altimetric variability of more than 1000 m, coupled with considerable spatial variability (the results are similar if we consider the AAR or AABR methods, or a combination of the two values, where available). This wide range of ELA variability reflects the values reconstructed for the LGM on the entire Alpine chain, as proposed by Kuhlemann et al. (2008) and by Višnjević et al. (2020), who indicate a range of about 600 m and 1000 m, respectively. The ELAs reconstructed for the Egesen glaciers in the Gran Paradiso are among the highest values recorded along the entire Alpine chain.

It is well-known that the position of the ELA is closely related to the climatic parameters of the area under consideration, and paleo-ELA reconstruction provides relevant paleoclimatic information in this regard. Considering that the precipitation amounts during the Egesen and the LIA are close to present-day precipitations and assuming a standard modern average lapse-rate of 0.65 °C/100 m, our data have led to estimate that the Egesen phase may have been characterized by a mean annual temperature of ca. 1.5/1.4 °C lower than the LIA (considering the weighted mean ELA calculated with AAR and AABR, respectively), and about 2.6/2.2 °C lower than in 2006 CE. Moreover, the ELA between the maximum LIA position and 2006 CE has risen even further (ca. 163 ± 6 m/126 ± 7 m considering AAR/AABR). Despite the unsteady state condition of the Gran Paradiso glaciers in 2006 CE, the temperatures during the LIA would have been at least 1.1/0.8 °C lower than in 2006 CE. If we apply the standard modern average lapse-rate of 0.6–0.8 °C/100 m used by Braithwaite and Zeng (2000) to estimate the sensitivity of glacier mass balance to temperature change in the Swiss Alps, the mean temperature during the Egesen phase would have been lower than the LIA by 1.4/1.3 °C to 1.8/1.7 °C and lower than 2006 CE by 2.4/2.1 °C to 3.1/2.7 °C (considering the weighted mean ELA calculated with AAR and AABR, respectively).

To move further beyond these results, we should more realistically consider combined changes in temperature and precipitation. Indeed, the wide Egesen ELA variation with respect to the LGM in different sectors of the Alps seems to be related not only to temperature variations but, most likely, to changes in the precipitation amount (and possibly precipitation intensity and distribution in different seasons) and in the storm track, as highlighted also

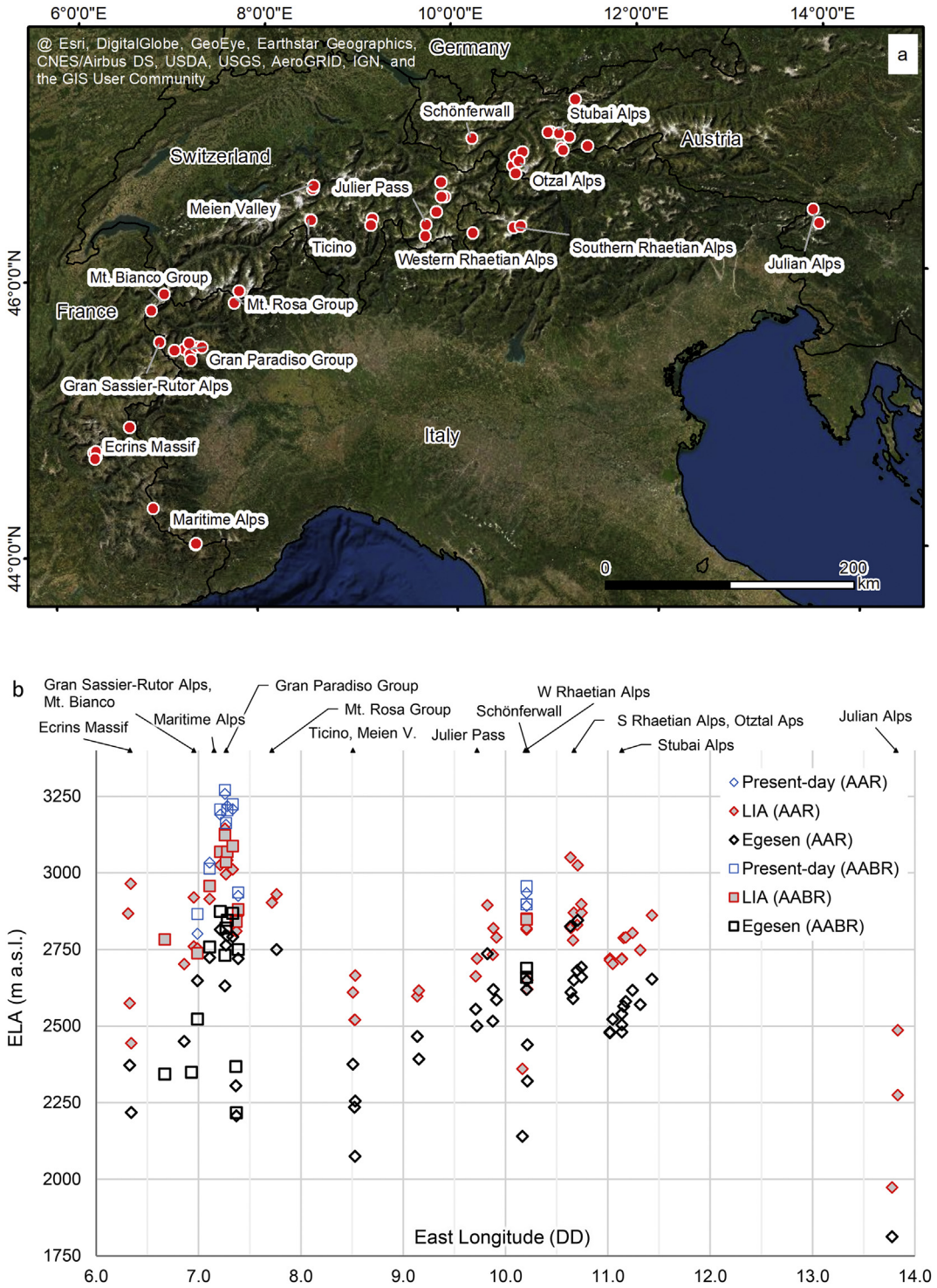

Fig. 8. Selected Alpine sites with Egesen moraines compared with the study area (a) and altitudinal distributions of ELA values (m a.s.l.) with respect to the Longitude (b). Gran Paradiso data from this work, other Egesen ELA values from literature (Gross et al., 1977; Kerschner, 1979; Porter and Orombelli, 1982; Sailer, 2001; Vanuzzo, 2001; Carturan and Seppi, 2007; Hormes et al., 2008; Cossart et al., 2012; Mautner, 2012; Scapozza et al., 2014; Ivy-Ochs, 2015; Colucci, 2016; Moran et al., 2016, 2017; Baroni et al., 2017; Federici et al., 2017; Kozamernik et al., 2018; Boxleitner et al., 2019b; Hofmann et al., 2019; Protin et al., 2019; Scotti et al., 2017; Spagnolo and Ribolini, 2019). For details, see Supplementary Material, Appendix A, Table A.5. (For interpretation of the references to colour in this figure legend, the reader is referred to the Web version of this article).

in the Northern Apennines during the LGM (Baroni et al., 2018). The spatial variation of precipitation in the Alpine Chain during the Egesen stadial is also evidenced by the ELA depression with respect to the LIA maximum position, as Gross et al. (1977) first pointed out in the Tyrolean Stubai Alps. The snow-line depression of the Egesen stadial was not constant and was larger in the wetter areas of the Northern Alps (300–320 m) compared to the drier and more continental Central Alps (180–220 m) (Gross et al., 1977; Kerschner et al., 2000).

As also evidenced by Protin et al. (2019), reconstructions of the

paleo-precipitations of specific sites are generally very rare in the Alps. Therefore, we tentatively reconstructed paleo-precipitations during the YD at the ELA elevations of the Egesen paleo-glaciers in the Gran Paradiso area, with independent proxy data available in the proximity of our study area (Chironomid assemblage at Lago Piccolo di Avigliana, Larocque and Finsinger, 2008; pollen studies at Laghi dell'Orgials, Ortu et al., 2008).

YD paleo-temperatures obtained at the Egesen ELAs (with AAR/AABR methods), ranging from about 0.4/0.0 °C to −19.4/−19.8 °C for the hottest (July) and the coldest (January) months, respectively (applying the average lapse-rate of 0.65 °C/100 m), allowed us to fit a sine function with amplitude equal to 9.9/9.9 °C and midline at −9.5/−9.9 °C, and to infer a mean YD summer temperature (June, July and August) equal to −0.62/−0.98 °C (at the Egesen ELAs, considering the AAR/AABR methods, respectively). At the elevation of the Egesen ELA, the values obtained were ca 5.4/5.4 °C, 4.2/4.2 °C and 9.2/9.2 °C lower than the present-day (mean over the 30-year period 1961–1990) summer temperature, T_{Jul} and T_{Jan}, respectively. If we speculatively apply the current lapse-rates calculated for the regional climatic equilibrium line altitude of glaciers in the European Alps (0.71 °C/100 m and 0.54 °C/100 m for the hottest and coldest months, respectively; Zemp et al., 2007), we obtain temperatures equal to −1.0/−1.4 °C and −18.8/−19.1 °C at the Egesen ELAs in the Gran Paradiso Group, considering the AAR/AABR methods, respectively (Table 4).

Paleo-precipitation obtained with independent proxy records (Chironomids from Lago Piccolo di Avigliana and pollen from Laghi dell'Orgials) provided values comparable to the present-day precipitation amounts. Our results underline particularly dry conditions with values of about 827/746 mm yr^{-1} using the quadratic approximation of the precipitation equation (Ohmura and Boettcher, 2018) applied on the Egesen ELA summer temperatures (considering both the AAR and AABR methods). Even lower values can be obtained by applying the linear approximation of the precipitation equation (795/698 mm yr^{-1}), as proposed by Ohmura and Boettcher (2018).

On the basis of other data available for the European Alps derived from lacustrine proxy records (e.g. pollen, Chironomids, Heiri et al., 2011, 2014a, 2014b, Fig. 9), we tentatively reconstructed paleo-temperature and paleo-precipitation at the Egesen ELAs during the YD. Mean YD T_{jul} values are consistent with those from the Lago Piccolo di Avigliana.

Global paleo-climate models with high spatial resolution that consider orographic predictors (including winds, valley aspect, etc.) have been developed recently (Karger et al., 2017; Brown et al., 2018). They represent an independent and reliable source to analyse the spatial variability of paleo-climatic parameters and their connection with ELA reconstructions (James et al., 2019). Our reconstructions of paleo-climatic parameters at the Egesen ELAs during the YD fit with the paleo-climatic condition models that show mean YD precipitation and temperature values in the entire study area of Gran Paradiso of about 911 ± 120 mm/yr and of −5.8 ± 2.2 °C, respectively (Karger et al., 2017; Brown et al., 2018). On the other hand, the LGM paleo-climatic model (Fordham et al., 2017; Karger et al., 2017; Brown et al., 2018) shows that − compared to the YD − the Gran Paradiso Group area was characterized by lower temperatures (as mean of about −6.1 °C for the Δpaleo-T between LGM-YD) and higher mean precipitation values, higher than 1300 mm/yr in the LGM (with mean Δpaleo-P LGM-YD >210 ± 124 mm/yr; data derived from PaleoClim datasets, Karger et al., 2017; Brown et al., 2018).

Although mean paleo-temperatures were clearly lower than present-day temperatures, the spatial correlation between ELAs and YD temperatures cannot be clearly identified along the Alpine chain (Fig. 9a).

Instead, the variability of the ELA during the Egesen and the LIA (Gennaro, 2020) seems to be mainly correlated to different precipitation patterns, considering both the current (Isotta et al., 2014) and the YD precipitation distribution (Kerschner, 1980, 2005; Kerschner et al., 2000; Fordham et al., 2017; Karger et al., 2017; Brown et al., 2018).

Egesen ELAs show considerable variability within the YD precipitation pattern (Fig. 9b): the highest reconstructed ELA values for the Egesen phase were recorded in the Ortles Group (southern Rhaetian Alps) and in the Gran Paradiso Group, both located in relatively drier areas considering both the YD-precipitation pattern (from PaleoClim, Fordham et al., 2017; Karger et al., 2017; Brown et al., 2018) and the present-day precipitation pattern (Isotta et al., 2014). The lowest Egesen ELAs were collected for relatively wetter areas like the Julian Alps (Kozamernik et al., 2018).

This altitudinal distribution of the ELA values along the Alpine Chain remained practically unvaried even during the LIA maximum glacier extension, although obviously related to higher ELA values (Fig. 8 and references in caption).

6. Conclusions

Glaciers hosted in the Gran Paradiso Group are sensitive indicators of recent and ongoing climatic changes, and also of past climatic variations at least since the Late Pleistocene. Landscape analysis, glacial geological survey, ^{10}Be exposure ages (first obtained in the Gran Paradiso Group), coupled with the reconstruction of glacier paleo-topography for the reconstruction of ELA variations (ΔELAs), allowed us to chronologically constrain and characterize the last Lateglacial glacier advance phase occurred in this key sector of the Western Alps. Our data supply valuable results supporting the attribution of the last Lateglacial phase to the Egesen stadial, substantially correlated to the YD, as widely recognized for many other Alpine locations (Ivy-Ochs et al., 2008; Moran et al., 2016; Baroni et al., 2017, and references therein).

Egesen ELAs (AAR/AABR) on the Gran Paradiso area are among the highest values recorded along the Alpine Chain and, together with the ΔELA values provided here, they have made it possible to infer the associated ΔT. We provided ΔTs associated with specific ΔELA values, by assuming unchanged precipitation values compared to the current ones. By coupling the YD ELAs obtained for this Alpine sector with independent proxy records, we tentatively inferred the main paleo-climatic parameters (YD paleo-T and YD paleo-P) characterizing the Egesen ELA. The consistency of these quantitative results, which well fit with recent paleo-precipitation distribution models (Fordham et al., 2017; Karger et al., 2017; Brown et al., 2018), have allowed us to infer that the current relatively dry conditions of the Gran Paradiso area were established after the LGM during Termination I, at least since the Egesen stadial. Our conclusions suggest that the atmospheric circulation during the YD was driven by a positive North Atlantic Oscillation. Indeed, it was hypothesized that, at least during the YD, the westerlies passing over the colder and potentially ice-covered North Atlantic Sea would accumulate less heat and moisture, resulting in a cooler and drier effect on western Europe (Brauer et al., 2008). Moreover, our results are consistent with a strong positive modeled Artic Oscillation index during the YD, induced by lower sea-level pressure over the Greenland-Artic region coupled with higher sea-level pressures over the NE Atlantic, which implied atmospheric blocking conditions (Schenk et al., 2018). Positive phases of the Artic Oscillation, like the North Atlantic Oscillation, brought less moisture to southern Europe, causing negative extreme precipitation winter anomalies (Tabari and Willems, 2018).

The quantitative results presented here have allowed us to provide not only the first chronological constraints of the Egesen

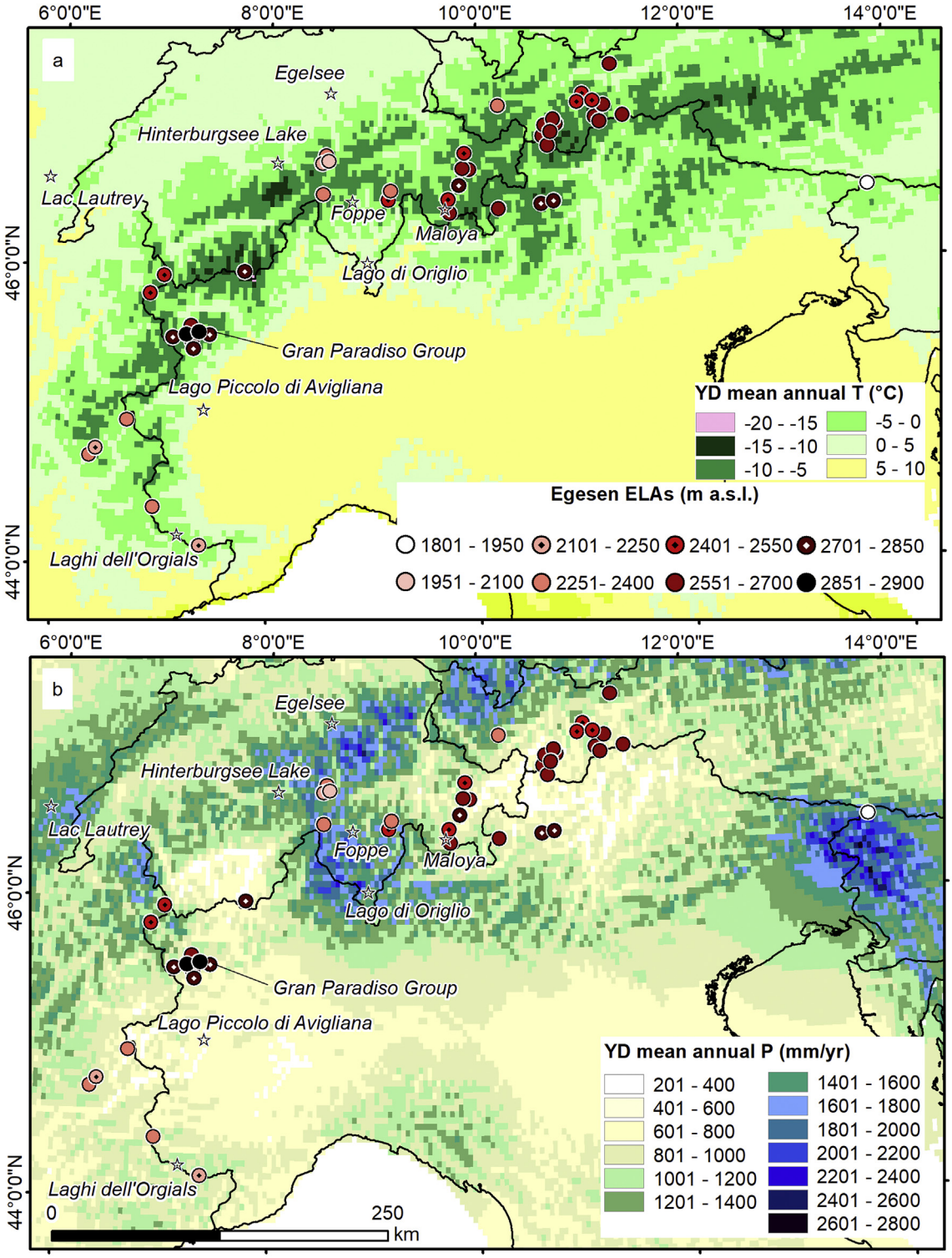

Fig. 9. ELA values (m a.s.l.) reconstructed for the Egesen stadial in the Gran Paradiso Group (this paper) and in other studied sites in the Alps, compared with the distribution of: a) paleo-temperatures (°C), and b) paleo-precipitations (mm/yr) modeled for the YD (from PaleoClim, Fordham et al., 2017; Karger et al., 2017; Brown et al., 2018). Egesen ELA values references as in Fig. 8. Stars indicate site furnishing T_{jul} temperature (°C) from Larocque and Finsinger (2008) and Heiri et al. (2014b); and T_{jan} temperature (°C) from Ortu et al. (2008). (For interpretation of the references to colour in this figure legend, the reader is referred to the Web version of this article).

stadial in this area, but also quantitative paleo-climatic data able to tentatively reconstruct temperature and precipitation at the ELA with seasonal resolution during the Egesen, suitable for modelling climatic changes that characterized Termination I at the southern margin of the Alps. Finally, the reconstructed paleotemperature and paleoprecipitation during the Egesen stadial in the Gran Paradiso Group furnish new data for implementing the model of atmospheric circulation in Europe during the YD (Rea et al., 2020).

Authors statements

Carlo Baroni: Conception and design of study, acquisition of data, Drafting the manuscript, revising the manuscript critically for important intellectual content. **Simona Gennaro**: acquisition of data, analysis and/or interpretation of data, Drafting the manuscript. **Maria Cristina Salvatore**: Conception and design of study, acquisition of data, Drafting the manuscript, revising the manuscript critically for important intellectual content. **Susan Ivy-Ochs**: analysis and/or interpretation of data, revising the manuscript critically for important intellectual content. **Marcus Christl**: analysis and/or interpretation of data. **Riccardo Cerrato**: software: RC coded the python ArcGIS tool for ELA calculation. **Giuseppe Orombelli:** revising the manuscript critically for important intellectual content.

Declaration of competing interest

The authors declare that they have no known competing financial interests or personal relationships that could have appeared to influence the work reported in this paper.

Acknowledgements

This study was funded by the University of Pisa research grants (Fondi Ateneo C. Baroni and M.C. Salvatore 2016–2019; PRA-2020_60, "*La Terminazione I. Variazioni ambientali/paleoclimatiche intercorse nel periodo 25–11 ka*", Resp. A. Ribolini) and by the PhD Course in Earth Sciences of the University of Pisa, 32nd cycle.

CB, SG and MCS conducted glacial-geological and geomorphological surveys, and field sampling. SG and MCS organized the database and processed the GIS data. SG prepared the samples for surface exposure dating conducted at the ETH Laboratory for Ion Beam Physics by SIO and MC. RC coded the python ArcGIS tool for ELA calculation. CB, SG, GO, and MCS prepared the preliminary version of the manuscript. All authors contributed to the final version of the text.

We thank all members of the Ion Beam Physics group and Stefano Casale for their support during sample preparation and AMS measurements.

We wish to thank the editor Prof. Colm O'Cofaigh and the two anonymous reviewers for careful and valuable comments and suggestions, which allowed to improve the manuscript.

Appendix A. Supplementary data

Supplementary data to this article can be found online at https://doi.org/10.1016/j.quascirev.2021.106815.

References

Anderson, R.S., Anderson, L.S., Armstrong, W.H., Rossi, M.W., Crump, S.E., 2018. Glaciation of alpine valleys: the glacier—debris-covered glacier—rock glacier continuum. Geomorphology 311, 127–142. https://doi.org/10.1016/j.geomorph.2018.03.015.

Auer, I., Böhm, R., Jurkovic, A., Lipa, W., Orlik, A., Potzmann, R., Schöner, W., Ungersböck, M., Matulla, C., Briffa, K., Jones, P., Efthymiadis, D., Brunetti, M., Nanni, T., Maugeri, M., Mercalli, L., Mestre, O., Moisselin, J.-M., Begert, M., Müller-Westermeier, G., Kveton, V., Bochnicek, O., Šťastný, P., Lapin, M., Szalai, S., Szentimrey, T., Cegnar, T., Dolinar, M., Gajic-Capka, M., Zaninović, K., Majstorović, Ž., Nieplova, E., 2007. HISTALP—historical instrumental climatological surface time series of the Greater Alpine Region. Int. J. Climatol. 27, 17–46. https://doi.org/10.1002/joc.1377.

Balco, G., 2011. Contributions and unrealized potential contributions of cosmogenic-nuclide exposure dating to glacier chronology, 1990–2010. Quat. Sci. Rev. 30, 3–27. https://doi.org/10.1016/j.quascirev.2010.11.003.

Balco, G., Briner, J., Finkel, R.C., Rayburn, J.A., Ridge, J.C., Schaefer, J.M., 2009. Regional beryllium-10 production rate calibration for late-glacial northeastern North America. Quat. Geochronol. 4, 93–107. https://doi.org/10.1016/j.quageo.2008.09.001.

Balco, G., Stone, J.O., Lifton, N.A., Dunai, T.J., 2008. A complete and easily accessible means of calculating surface exposure ages or erosion rates from 10Be and 26Al measurements. Quat. Geochronol. 3, 174–195. https://doi.org/10.1016/j.quageo.2007.12.001.

Baroni, C., Carton, A., 1996. Geomorfologia dell'Alta val di Genova (gruppo dell'Adamello, Alpi Centrali). Geogr. Fis. Din. Quaternaria 19, 3–17.

Baroni, C., Carton, A., 1990. Variazioni oloceniche della Vedretta della Lobbia (gruppo dell'Adamello, Alpi Centrali). Geogr. Fis. Din. Quaternaria 13, 105–119.

Baroni, C., Casale, S., Salvatore, M.C., Ivy-Ochs, S., Christl, M., Carturan, L., Seppi, R., Carton, A., 2017. Double response of glaciers in the upper Peio valley (Rhaetian Alps, Italy) to the younger Dryas climatic deterioration. Boreas 46, 783–798. https://doi.org/10.1111/bor.12284.

Baroni, C., Guidobaldi, G., Salvatore, M.C., Christl, M., Ivy-Ochs, S., 2018. Last glacial maximum glaciers in the Northern Apennines reflect primarily the influence of southerly storm-tracks in the western Mediterranean. Quat. Sci. Rev. 197, 352–367. https://doi.org/10.1016/j.quascirev.2018.07.003.

Baroni, C., Martino, S., Salvatore, M.C., Scarascia Mugnozza, G., Schilirò, L., 2014. Thermomechanical stress-strain numerical modelling of deglaciation since the last glacial maximum in the Adamello group (Rhaetian Alps, Italy). Geomorphology 226, 278–299. https://doi.org/10.1016/j.geomorph.2014.08.013.

Beltrando, M., Compagnoni, R., Lombardo, B., 2010. Ultra-) High-pressure metamorphism and orogenesis: an Alpine perspective. Gondwana Res. 18, 147–166. https://doi.org/10.1016/j.gr.2010.01.009.

Beschel, R., 1958. Ricerche lichenometriche sulle morene del gruppo del Gran Paradiso. Nuovo G. Bot. Ital. 65, 538–591.

Boxleitner, M., Ivy-Ochs, S., Egli, M., Brandova, D., Christl, M., Dahms, D., Maisch, M., 2019a. The ^{10}Be deglaciation chronology of the Göschenertal, central Swiss Alps, and new insights into the Göschenen Cold Phases. Boreas 48, 867–878. https://doi.org/10.1111/bor.12394.

Boxleitner, M., Ivy-Ochs, S., Egli, M., Brandova, D., Christl, M., Maisch, M., 2019b. Lateglacial and early Holocene glacier stages - new dating evidence from the meiental in central Switzerland. Geomorphology 340, 15–31. https://doi.org/10.1016/j.geomorph.2019.04.004.

Braithwaite, R.J., Zhang, Y., 2000. Sensitivity of mass balance of five Swiss glaciers to temperature changes assessed by tuning a degree-day model. J. Glaciol. 46, 7–14. https://doi.org/10.3189/172756500781833511.

Brauer, A., Haug, G.H., Dulski, P., Sigman, D.M., Negendank, J.F.W., 2008. An abrupt wind shift in western Europe at the onset of the Younger Dryas cold period. Nat. Geosci. 1, 520–523. https://doi.org/10.1038/ngeo263.

Broecker, W.S., Denton, G.H., Edwards, R.L., Cheng, H., Alley, R.B., Putnam, A.E., 2010. Putting the Younger Dryas cold event into context. Quat. Sci. Rev. 29, 1078–1081. https://doi.org/10.1016/j.quascirev.2010.02.019.

Brooks, S.J., Heiri, O., 2013. Response of chironomid assemblages to environmental change during the early Late-glacial at Gerzensee, Switzerland. Palaeogeogr. Palaeoclimatol. Palaeoecol. 391, 90–98. https://doi.org/10.1016/j.palaeo.2012.10.022.

Brown, J.L., Hill, D.J., Dolan, A.M., Carnaval, A.C., Haywood, A.M., 2018. PaleoClim, high spatial resolution paleoclimate surfaces for global land areas. Sci. Data 5, 180254. https://doi.org/10.1038/sdata.2018.254.

Brunetti, M., Lentini, G., Maugeri, M., Nanni, T., Auer, I., Böhm, R., Schöner, W., 2009. Climate variability and change in the Greater Alpine Region over the last two centuries based on multi-variable analysis. Int. J. Climatol. 29, 2197–2225. https://doi.org/10.1002/joc.1857.

Carturan, L., Baroni, C., Becker, M., Bellin, A., Cainelli, O., Carton, A., Casarotto, C., Dalla Fontana, G., Godio, A., Martinelli, T., Salvatore, M.C., Seppi, R., 2013a. Decay of a long-term monitored glacier: Careser glacier (Ortles-Cevedale, European Alps). Cryosphere 7, 1819–1838. https://doi.org/10.5194/tc-7-1819-2013.

Carturan, L., Baroni, C., Carton, A., Cazorzi, F., Dalla Fontana, G., Delpero, C., Salvatore, M.C., Seppi, R., Zanoner, T., 2014. Reconstructing fluctuations of La Mare glacier (eastern Italian Alps) in the late Holocene: new evidence for a Little ice age maximum around 1600 AD. Geogr. Ann. Phys. Geogr. 96, 287–306. https://doi.org/10.1111/geoa.12048.

Carturan, L., Filippi, R., Seppi, R., Gabrielli, P., Notarnicola, C., Bertoldi, L., Paul, F., Rastner, P., Cazorzi, F., Dinale, R., Dalla Fontana, G., 2013b. Area and volume loss of the glaciers in the Ortles-Cevedale group (Eastern Italian Alps): controls and imbalance of the remaining glaciers. Cryosphere 7, 1339–1359. https://doi.org/10.5194/tc-7-1339-2013.

Carturan, L., Seppi, R., 2007. Recent mass balance results and morphological evolution of Careser glacier (Central Alps). Geogr. Fis. Din. Quaternaria 30, 33–42.

Chenet, M., Brunstein, D., Jomelli, V., Roussel, E., Rinterknecht, V., Mokadem, F., Biette, M., Robert, V., Léanni, L., 2016. 10Be cosmic-ray exposure dating of moraines and rock avalanches in the Upper Romanche valley (French Alps): evidence of two glacial advances during the Late Glacial/Holocene transition. Quat. Sci. Rev. 148, 209–221. https://doi.org/10.1016/j.quascirev.2016.07.025.

Chmeleff, J., von Blanckenburg, F., Kossert, K., Jakob, D., 2010. Determination of the 10Be half-life by multicollector ICP-MS and liquid scintillation counting. Beam Interactions with Materials and Atoms 268 (2), 192–199. https://doi.org/10.1016/j.nimb.2009.09.012.

Christl, M., Vockenhuber, C., Kubik, P.W., Wacker, L., Lachner, J., Alfimov, V., Synal, H.-A., 2013. The ETH Zurich AMS facilities: Performance parameters and reference materials. Nucl. Instrum. Methods Phys. Res. Sect. B Beam Interact. Mater. Atoms 294, 29–38. https://doi.org/10.1016/j.nimb.2012.03.004.

Codilean, A.T., 2006. Calculation of the cosmogenic nuclide production topographic shielding scaling factor for large areas using DEMs. Earth Surf. Process.

Landforms 31, 785–794. https://doi.org/10.1002/esp.1336.
Colucci, R.R., 2016. Geomorphic influence on small glacier response to post-Little Ice Age climate warming: Julian Alps, Europe. Earth Surf. Process. Landforms 41, 1227–1240. https://doi.org/10.1002/esp.3908.
Cossart, E., Fort, M., Bourlès, D., Braucher, R., Perrier, R., Siame, L., 2012. Deglaciation pattern during the Lateglacial/Holocene transition in the southern French Alps. Chronological data and geographical reconstruction from the Clarée Valley (upper Durance catchment, southeastern France). Palaeogeogr. Palaeoclimatol. Palaeoecol. 315–316, 109–123. https://doi.org/10.1016/j.palaeo.2011.11.017.
Crespi, A., Brunetti, M., Lentini, G., Maugeri, M., 2018. 1961-1990 high-resolution monthly precipitation climatologies for Italy. Int. J. Climatol. 38, 878–895. https://doi.org/10.1002/joc.5217.
Dal Piaz, G.V., Gianotti, F., Monopoli, B., Pennacchioni, G., Tartarotti, P., Schiavo, A., 2008. Carta Geologica d'Italia alla scala 1:50000 e Note illustrative. Foglio 91 Chatillon. ISPRA - Istituto Superiore per la Protezione e la Ricerca Ambientale, Rome.
Di Nicola, L., Strasky, S., Schlüchter, C., Salvatore, M.C., Akçar, N., Kubik, P.W., Christl, M., Kasper, H.U., Wieler, R., Baroni, C., 2009. Multiple cosmogenic nuclides document complex Pleistocene exposure history of glacial drifts in Terra Nova Bay (northern Victoria Land, Antarctica). Quat. Res. 71, 83–92. https://doi.org/10.1016/j.yqres.2008.07.004.
EEA, 2009. Regional climate change and adaptation. Rep. EEA No. 8/2009 8 148. https://doi.org/10.2800/12552.
Elter, G., 1987. Carte géologique de la Vallée d'Aoste, échelle 1:100.000. [Geological Map of the Aosta Valley].
Favilli, F., Egli, M., Brandova, D., Ivy-Ochs, S., Kubik, P., Cherubini, P., Mirabella, A., Sartori, G., Giaccai, D., Haeberli, W., 2009. Combined use of relative and absolute dating techniques for detecting signals of Alpine landscape evolution during the late Pleistocene and early Holocene. Geomorphology 112, 48–66. https://doi.org/10.1016/j.geomorph.2009.05.003.
Federici, P.R., Granger, D.E., Pappalardo, M., Ribolini, A., Spagnolo, M., Cyr, A.J., 2008. Exposure age dating and equilibrium line altitude reconstruction of an egesen moraine in the Maritime Alps, Italy. Boreas 37, 245–253. https://doi.org/10.1111/j.1502-3885.2007.00018.x.
Federici, P.R., Ribolini, A., Spagnolo, M., 2017. Glacial history of the Maritime Alps from the last glacial maximum to the Little ice age. Geol. Soc. London, Spec. Publ. 433, 137–159. https://doi.org/10.1144/SP433.9.
Fischer, A., 2011. Comparison of direct and geodetic mass balances on a multi-annual time scale. Cryosphere 5, 107–124. https://doi.org/10.5194/tc-5-107-2011.
Fischer, M., Huss, M., Hoelzle, M., 2015. Surface elevation and mass changes of all Swiss glaciers 1980-2010. Cryosphere 9, 525–540. https://doi.org/10.5194/tc-9-525-2015.
Fordham, D.A., Saltré, F., Haythorne, S., Wigley, T.M.L., Otto-Bliesner, B.L., Chan, K.C., Brook, B.W., 2017. PaleoView: a tool for generating continuous climate projections spanning the last 21 000 years at regional and global scales. Ecography (Cop 40, 1348–1358. https://doi.org/10.1111/ecog.03031.
Furrer, G., Burga, C., Gamper, M., Holzhauser, H.-P., Maisch, M., 1987. Zur Gletscher-, Vegetations- und Klimageschichte der Schweiz seit der Späteiszeit. Geograph. Helv. 42, 61–91. https://doi.org/10.5194/gh-42-61-1987.
Gardent, M., Rabatel, A., Dedieu, J.P., Deline, P., 2014. Multitemporal glacier inventory of the French Alps from the late 1960s to the late 2000s. Global Planet. Change 120, 24–37. https://doi.org/10.1016/j.gloplacha.2014.05.004.
Garzena, D., Fratianni, S., Acquaotta, F., 2015. Temperature analysis on the northwestern Italian Alps through the use of satellite images and ground-based meteorological stations. In: Engineering Geology for Society and Territory, vol. 1. Springer International Publishing, Cham, pp. 77–80. https://doi.org/10.1007/978-3-319-09300-0_15.
Gasco, I., Gattiglio, M., Borghi, A., 2009. Structural evolution of different tectonic units across the Austroalpine–Penninic boundary in the middle Orco Valley (western Italian Alps). J. Struct. Geol. 31, 301–314. https://doi.org/10.1016/j.jsg.2008.11.007.
Gennaro, S., 2020. Glaciers of the Gran Paradiso Group as Indicator of Lateglacial and Holocene Climatic Changes in the Western Alps. PhD Thesis. University of Pisa.
Gianotti, F., Forno, M.G., Ivy-Ochs, S., Kubik, P.W., 2008. New chronological and stratigraphical data on the Ivrea amphitheatre (Piedmont, NW Italy). Quat. Int. 190, 123–135. https://doi.org/10.1016/j.quaint.2008.03.001.
Gianotti, F., Forno, M.G., Ivy-Ochs, S., Monegato, G., Pini, R., Ravazzi, C., 2015. Stratigraphy of the Ivrea morainic amphitheatre (NW Italy): an updated synthesis. Alp. Mediterr. Quat. 28, 29–58.
GNGFG-CNR, 1986. Ricerche geomorfologiche nell'alta Val di Peio (Gruppo del Cevedale). Geogr. Fis. Din. Quaternaria 9, 137–191.
Gross, G. von, Kerschner, H., Patzelt, G., 1977. Methodische Untersuchungen über die Schneegrenze in alpinen Gletschergebieten. Zeitschrift für Gletscherkd. und Glazialgeol. 12, 223–251.
Heiri, O., Brooks, S.J., Birks, H.J.B., Lotter, A.F., 2011. A 274-lake calibration data-set and inference model for chironomid-based summer air temperature reconstruction in Europe. Quat. Sci. Rev. 30, 3445–3456. https://doi.org/10.1016/j.quascirev.2011.09.006.
Heiri, O., Brooks, S.J., Renssen, H., Bedford, A., Hazekamp, M., Ilyashuk, B., Jeffers, E.S., Lang, B., Kirilova, E., Kuiper, S., Millet, L., Samartin, S., Toth, M., Verbruggen, F., Watson, J.E., Van Asch, N., Lammertsma, E., Amon, L., Birks, H.J.B.H., Birks, H.J.B.H., Mortensen, M.F., Hoek, W.Z., Magyari, E., Munõz Sobrino, C., Seppä, H., Tinner, W., Tonkov, S., Veski, S., Lotter, A.F., 2014a. Validation of climate model-inferred regional temperature change for late-glacial Europe. Nat. Commun. 5, 1–7. https://doi.org/10.1038/ncomms5914.
Heiri, O., Koinig, K.A., Spötl, C., Barrett, S., Brauer, A., Drescher-Schneider, R., Gaar, D., Ivy-Ochs, S., Kerschner, H., Luetscher, M., Moran, A., Nicolussi, K., Preusser, F., Schmidt, R., Schoeneich, P., Schwörer, C., Sprafke, T., Terhorst, B., Tinner, W., 2014b. Palaeoclimate records 60-8 ka in the Austrian and Swiss Alps and their forelands. Quat. Sci. Rev. 106, 186–205. https://doi.org/10.1016/j.quascirev.2014.05.021.
Heuberger, H., 1968. Die Alpengletscher im Spät- und Postglazial: eine chronologische Übersicht. Quat. Sci. J. 19, 270–275. https://doi.org/10.3285/eg.19.1.24.
Hofmann, F.M., Alexanderson, H., Schoeneich, P., Mertes, J.R., Léanni, L., , Aster Team (Georges Aumaitre Didier L, Bourles, K.K., 2019. Post-Last Glacial Maximum glacier fluctuations in the southern Écrins massif (westernmost Alps): insights from 10Be cosmic ray exposure dating. Boreas 48, 1019–1041. https://doi.org/10.1111/bor.12405.
Hormes, A., Ivy-Ochs, S., Kubik, P.W., Ferreli, L., Michetti, M.A., 2008. 10Be exposure ages of a rock avalanche and a late glacial moraine in Alta Valtellina, Italian Alps. Quat. Int. 190, 136–145. https://doi.org/10.1016/j.quaint.2007.06.036.
Huss, M., 2013. Density assumptions for converting geodetic glacier volume change to mass change. Cryosphere Discuss. 7, 219–244. https://doi.org/10.5194/tcd-7-219-2013.
IPCC, 2013. Climate Change 2013: the Physical Science Basis. Contribution of Working Group I to the Fifth Assessment Report of the Intergovernmental Panel on Climate Change. Cambridge University Press, Cambridge, United Kingdom and New York, NY, USA.
IPCC, 2007. Climate Change 2007: Synthesis Report. Contribution of Working Groups I, II and III to the Fourth Assessment Report of the Intergovernmental Panel on Climate Change. IPCC, Geneva, Switzerland.
Isotta, F.A., Frei, C., Weilguni, V., Perčec Tadić, M., Lassègues, P., Rudolf, B., Pavan, V., Cacciamani, C., Antolini, G., Ratto, S.M., Munari, M., Micheletti, S., Bonati, V., Lussana, C., Ronchi, C., Panettieri, E., Marigo, G., Vertačnik, G., 2014. The climate of daily precipitation in the Alps: development and analysis of a high-resolution grid dataset from pan-Alpine rain-gauge data. Int. J. Climatol. 34, 1657–1675. https://doi.org/10.1002/joc.3794.
Ivy-Ochs, S., 2015. Glacier variations in the European Alps at the end of the last glaciation. Cuadernos Invest. Geogr. 41, 295. https://doi.org/10.18172/cig.2750.
Ivy-Ochs, S., Kerschner, H., Maisch, M., Christl, M., Kubik, P.W., Schlüchter, C., 2009. Latest Pleistocene and Holocene glacier variations in the European Alps. Quat. Sci. Rev. 28, 2137–2149. https://doi.org/10.1016/j.quascirev.2009.03.009.
Ivy-Ochs, S., Kerschner, H., Reuther, A., Maisch, M., Sailer, R., Schaefer, J., Kubik, P.W., Synal, H.-A., Schlüchter, C., 2006. The timing of glacier advances in the northern European Alps based on surface exposure dating with cosmogenic ^{10}Be, ^{26}Al, ^{36}Cl, and ^{21}Ne. In: Situ-Produced Cosmogenic Nuclides and Quantification of Geological Processes. Geological Society of America, pp. 43–60. https://doi.org/10.1130/2006.2415(04.
Ivy-Ochs, S., Kerschner, H., Reuther, A., Preusser, F., Heine, K., Maisch, M., Kubik, P.W., Schlüchter, C., 2008. Chronology of the last glacial cycle in the European Alps. J. Quat. Sci. 23, 559–573. https://doi.org/10.1002/jqs.1202.
Ivy-Ochs, S., Kober, F., 2008. Surface exposure dating with cosmogenic nuclides. Quat. Sci. J. 57, 179–209. https://doi.org/10.3285/eg.57.1-2.7.
James, W.H.M., Carrivick, J.L., Quincey, D.J., Glasser, N.F., 2019. A geomorphology based reconstruction of ice volume distribution at the Last Glacial Maximum across the Southern Alps of New Zealand. Quat. Sci. Rev. 219, 20–35. https://doi.org/10.1016/j.quascirev.2019.06.035.
Karger, D.N., Conrad, O., Böhner, J., Kawohl, T., Kreft, H., Soria-Auza, R.W., Zimmermann, N.E., Linder, H.P., Kessler, M., 2017. Climatologies at high resolution for the earth's land surface areas. Sci. Data 4, 170122. https://doi.org/10.1038/sdata.2017.122.
Kerschner, H., 2009. Gletscher und Klima im Alpinen Spätglazial und frühen Holozän. In: Schmidt, R., Matulla, C., Psenner, R. (Eds.), Klimawandel in Österreich. Die Letzten 20.000 Jahre Und Ein Blick Voraus, Alpine Space - Man & Environment, vol. 6. Innsbruck University Press, pp. 5–26.
Kerschner, H., 2005. Glacier-climate models as Palaeoclimatic information sources: examples from the alpine younger Dryas period. In: Huber, U.M., Bugmann, H.K.M., Reasoner, M. (Eds.), Global Change and Mountain Regions. Advances in Global Change Research, vol. 23. Springer, Dordrecht, pp. 73–81. https://doi.org/10.1007/1-4020-3508-X_8.
Kerschner, H., 1980. Outlines of the climate during the egesen advance (younger Dryas, 11 000 - 10 000 BP) in the central Alps of the western Tyrol, Austria. Zeitschrift fur Gletscherkd. und Glazialgeol. 16, 229–240.
Kerschner, H., 1979. Zur Rekonstruktion eines spätglazialen Gletscherstandes mit Hilfe eines rechnerisch ermittelten Zungenlängsprofiles. Zeitschrift für Gletscherkd. und Glazialgeol. 14, 119–123.
Kerschner, H., Kaser, G., Sailer, R., 2000. Alpine Younger Dryas glaciers as palaeo-precipitation gauges. Ann. Glaciol. 31, 80–84. https://doi.org/10.3189/172756400781820237.
Kohl, C., Nishiizumi, K., 1992. Chemical isolation of quartz for measurement of in-situ -produced cosmogenic nuclides. Geochem. Cosmochim. Acta 56, 3583–3587. https://doi.org/10.1016/0016-7037(92)90401-4.
Korschinek, G., Bergmaier, A., Faestermann, T., Gerstmann, U.C., Knie, K., Rugel, G., Wallner, A., Dillmann, T., Dollinger, G., von Gostomski, Ch.L., Kossert, K., Maiti, M., Poutivtsev, M., Remmert, A., 2010. A new value for the half-life of 10Be by Heavy-Ion Elastic Recoil Detection and liquid scintillation counting. Nuclear Instruments and Methods in Physics Research, Section B: Beam

Interactions with Materials and Atoms 268 (2), 187–191. https://doi.org/10.1016/j.nimb.2009.09.020.
Kozamernik, E., Colucci, R.R., Stepišnik, U., Forte, E., Žebre, M., 2018. Spatial and climatic characterization of three glacial stages in the Upper Krnica Valley, SE European Alps. Quat. Int. 470, 67–81. https://doi.org/10.1016/j.quaint.2017.05.047.
Kuhlemann, J., Gachev, E., Gikov, A., Nedkov, S., Krumrei, I., Kubik, P., 2013. Glaciation in the Rila mountains (Bulgaria) during the last glacial maximum. Quat. Int. 293, 51–62. https://doi.org/10.1016/j.quaint.2012.06.027.
Kuhlemann, J., Rohling, E.J., Krumrei, I., Kubik, P., Ivy-Ochs, S., Kucera, M., 2008. Regional synthesis of mediterranean atmospheric circulation during the last glacial maximum. Science 321, 1338–1340. https://doi.org/10.1126/science.1157638.
Larocque, I., Finsinger, W., 2008. Late-glacial chironomid-based temperature reconstructions for Lago Piccolo di Avigliana in the southwestern Alps (Italy). Palaeogeogr. Palaeoclimatol. Palaeoecol. 257, 207–223. https://doi.org/10.1016/j.palaeo.2007.10.021.
Le Bayon, B., Ballèvre, M., 2006. Deformation history of a subducted continental crust (Gran Paradiso, Western Alps): continuing crustal shortening during exhumation. J. Struct. Geol. 28, 793–815. https://doi.org/10.1016/j.jsg.2006.02.009.
Li, Y., 2018. Determining topographic shielding from digital elevation models for cosmogenic nuclide analysis: a GIS model for discrete sample sites. J. Mt. Sci. 15, 939–947. https://doi.org/10.1007/s11629-018-4895-4.
Li, Y., 2013. Determining topographic shielding from digital elevation models for cosmogenic nuclide analysis: a GIS approach and field validation. J. Mt. Sci. 10, 355–362. https://doi.org/10.1007/s11629-013-2564-1.
Lowe, J.J., Rasmussen, S.O., Björck, S., Hoek, W.Z., Steffensen, J.P., Walker, M.J.C., Yu, Z., 2008. Synchronisation of palaeoenvironmental events in the North Atlantic region during the Last Termination: a revised protocol recommended by the INTIMATE group. Quat. Sci. Rev. 27, 6–17. https://doi.org/10.1016/j.quascirev.2007.09.016.
Lucchesi, S., Bertotto, S., Chiarle, M., Fioraso, G., Giardino, M., Nigrelli, G., 2019. Little Ice Age glacial systems and related natural instability processes in the Orco Valley (North-Western Italy). J. Maps 15, 142–152. https://doi.org/10.1080/17445647.2018.1564382.
Lucchesi, S., Fioraso, G., Bertotto, S., Chiarle, M., 2014. Little ice age and contemporary glacier extent in the western and South-western piedmont Alps (north-western Italy). J. Maps 10, 409–423. https://doi.org/10.1080/17445647.2014.880226.
Mackintosh, A.N., Anderson, B.M., Pierrehumbert, R.T., 2017. Reconstructing climate from glaciers. Annu. Rev. Earth Planet Sci. 45, 649–680. https://doi.org/10.1146/annurev-earth-063016-020643.
Maisch, M., 1982. Zur Gletscher- und Klimageschichte des alpinen Spätglazials. Geograph. Helv. 37, 93–104. https://doi.org/10.5194/gh-37-93-1982.
Mangerud, J., Andersen, S.T., Berglund, B.E., Donner, J.J., 1974. Quaternary stratigraphy of Norden, a proposal for terminology and classification. Boreas 3 (3), 109–126. https://doi.org/10.1111/j.1502-3885.1974.tb00669.x.
Manzotti, P., Le Carlier De Veslud, C., Le Bayon, B., Ballèvre, M., 2014. Petro-structural map of the money unit (gran Paradiso massif, Valnontey valley, western Alps). J. Maps 10, 324–340. https://doi.org/10.1080/17445647.2013.866912.
Marazzi, S., 2005. Atlante orografico delle Alpi: SOIUSA: suddivisione orografica internazionale unificata del sistema alpino, Quaderni di cultura alpina.
Mautner, P., 2012. Späteiszeitliche Gletscherstände im Platzertal, westliche Ötztaler Alpen (M.Sc Thesis). Universität Innsbruck.
Mayr, F., Heuberger, H., 1968. Type areas of late glacial and post-glacial deposits in Tyrol, eastern Alps. In: Richmond, G.M. (Ed.), Glaciation of the Alps, Series in Earth Sciences, vol. 7. University of Colorado Studies, pp. 143–165.
Moran, A.P., Ivy-Ochs, S., Schuh, M., Christl, M., Kerschner, H., 2016. Evidence of central Alpine glacier advances during the Younger Dryas–early Holocene transition period. Boreas 45, 398–410. https://doi.org/10.1111/bor.12170.
Moran, A.P., Ivy Ochs, S., Christl, M., Kerschner, H., 2017. Exposure dating of a pronounced glacier advance at the onset of the late-Holocene in the central Tyrolean Alps. Holocene 27, 1350–1358. https://doi.org/10.1177/0959683617690589.
Mortara, G., Orombelli, G., Pelfini, M., Tellini, C., 1992. Suoli e suoli sepolti olocenici per la datazione di eventi geomorfologici in ambiente alpino: Alcuni esempi tratti da indagini preliminari in Val d'Aosta. Quat 5, 135–146.
Nishiizumi, K., Imamura, M., Caffee, M.W., Southon, J.R., Finkel, R.C., McAninch, J., 2007. Absolute calibration of 10Be AMS standards. Nuclear Instruments and Methods in Physics Research, Section B: Beam Interactions with Materials and Atoms 258 (2), 403–413. https://doi.org/10.1016/j.nimb.2007.01.297.
Oerlemans, J., 2001. Glaciers and Climate Change. CRC Press, Tylor and Francis Group, Rotterdam.
Ohmura, A., Boettcher, M., 2018. Climate on the equilibrium line altitudes of glaciers: theoretical background behind Ahlmann's P/T diagram. J. Glaciol. 64, 489–505. https://doi.org/10.1017/jog.2018.41.
Orombelli, G., 2011. Holocene mountain glacier fluctuations: a global overview. Geogr. Fis. Din. Quaternaria 34, 17–24. https://doi.org/10.4461/GFDQ.2011.34.2.
Ortu, E., Peyron, O., Bordon, A., de Beaulieu, J.L., Siniscalco, C., Caramiello, R., 2008. Lateglacial and Holocene climate oscillations in the South-western Alps: an attempt at quantitative reconstruction. Quat. Int. 190, 71–88. https://doi.org/10.1016/j.quaint.2008.04.004.
Osmaston, H., 2005. Estimates of glacier equilibrium line altitudes by the Area×Altitude, the Area×Altitude balance ratio and the Area×Altitude balance index methods and their validation. Quat. Int. 138–139, 22–31. https://doi.org/10.1016/j.quaint.2005.02.004.
Palacios, D., Stokes, C.R., Phillips, F.M., Clague, J.J., Alcalá-Reygosa, J., Andrés, N., Angel, I., Blard, P.-H., Briner, J.P., Hall, B.L., Dahms, D., Hein, A.S., Jomelli, V., Mark, B.G., Martini, M.A., Moreno, P., Riedel, J., Sagredo, E., Stansell, N.D., Vázquez-Selem, L., Vuille, M., Ward, D.J., 2020. The deglaciation of the Americas during the last glacial termination. Earth Sci. Rev. 203, 103113. https://doi.org/10.1016/j.earscirev.2020.103113.
Paul, F., Barry, R., Cogley, G., Frey, H., Haeberli, W., Ohmura, A., Ommanney, C.S.L., Raup, B., Rivera, A., Zemp, M., 2010. Guidelines for the Compilation of Glacier Inventory Parameters from Digital Sources. World Glacier Monitoring Service, Zürich.
Paul, F., Barry, R.G., Cogley, J.G., Frey, H., Haeberli, W., Ohmura, A., Ommanney, C.S.L., Raup, B., Rivera, A., Zemp, M., 2009. Recommendations for the compilation of glacier inventory data from digital sources. Ann. Glaciol. 50, 119–126. https://doi.org/10.3189/172756410790595778.
Pellitero, R., Rea, B.R., Spagnolo, M., Bakke, J., Hughes, P., Ivy-Ochs, S., Lukas, S., Ribolini, A., 2015. A GIS tool for automatic calculation of glacier equilibrium-line altitudes. Comput. Geosci. 82, 55–62. https://doi.org/10.1016/j.cageo.2015.05.005.
Piana, F., Fioraso, G., Irace, A., Mosca, P., D'Atri, A., Barale, L., Falletti, P., Monegato, G., Morelli, M., Tallone, S., Vigna, G.B., 2017. Geology of Piemonte region (NW Italy, Alps–Apennines interference zone). J. Maps 13, 395–405. https://doi.org/10.1080/17445647.2017.1316218.
Polino, R., Bonetto, F., Carraro, F., Gianotti, F., Gouffon, Y., Malusà, M.G., Martin, S., Perello, P., Schiavo, A., 2015. Carta Geologica d'Italia alla scala 1:50000 e note illustrative. Foglio 90 Aosta. ISPRA - Istituto Superiore per la Protezione e la Ricerca Ambientale, Rome.
Porter, S.C., 1975. Equilibrium-line altitudes of late quaternary glaciers in the southern Alps, New Zealand. Quat. Res. 5, 27–47. https://doi.org/10.1016/0033-5894(75)90047-2.
Porter, S.C., Orombelli, G., 1982. Late-glacial ice advances in the western Italian Alps. Boreas 9, 125–140. https://doi.org/10.1111/j.1502-3885.1982.tb00530.x.
Poussin, C., Guigoz, Y., Palazzi, E., Terzago, S., Chatenoux, B., Giuliani, G., 2019. Snow cover evolution in the gran Paradiso national park, Italian Alps, using the earth observation data Cube. Data 4, 138. https://doi.org/10.3390/data4040138.
Protin, M., Schimmelpfennig, I., Mugnier, J.-L.J.-L., Ravanel, L., Le Roy, M., Deline, P., Favier, V., Buoncristiani, J.-F.J.-F., Aumaître, G., Bourlès, D.L., Keddadouche, K., Team, C.A., 2019. Climatic reconstruction for the younger dryas/early Holocene transition and the Little ice age based on paleo-extents of Argentière glacier (French Alps). Quat. Sci. Rev. 221, 105863. https://doi.org/10.1016/j.quascirev.2019.105863.
Rabatel, A., Letréguilly, A., Dedieu, J.-P., Eckert, N., 2013. Changes in glacier equilibrium-line altitude in the western Alps from 1984 to 2010: evaluation by remote sensing and modeling of the morpho-topographic and climate controls. Cryosphere 7, 1455–1471. https://doi.org/10.5194/tc-7-1455-2013.
Rasmussen, S.O., Bigler, M., Blockley, S.P., Blunier, T., Buchardt, S.L., Clausen, H.B., Cvijanovic, I., Dahl-Jensen, D., Johnsen, S.J., Fischer, H., Gkinis, V., Guillevic, M., Hoek, W.Z., Lowe, J.J., Pedro, J.B., Popp, T., Seierstad, I.K., Steffensen, J.P., Svensson, A.M., Vallelonga, P., Vinther, B.M., Walker, M.J.C., Wheatley, J.J., Winstrup, M., 2014. A stratigraphic framework for abrupt climatic changes during the Last Glacial period based on three synchronized Greenland ice-core records: refining and extending the INTIMATE event stratigraphy. Quat. Sci. Rev. 106, 14–28. https://doi.org/10.1016/j.quascirev.2014.09.007.
Rea, B.R., 2009. Defining modern day Area-Altitude Balance Ratios (AABRs) and their use in glacier-climate reconstructions. Quat. Sci. Rev. 28, 237–248. https://doi.org/10.1016/j.quascirev.2008.10.011.
Rea, B.R., Pellitero, R., Spagnolo, M., Hughes, P., Ivy-Ochs, S., Renssen, H., Ribolini, A., Bakke, J., Lukas, S., Braithwaite, R.J., 2020. Atmospheric circulation over Europe during the younger Dryas. Science Advances 6 (50), eaba4844. https://doi.org/10.1126/sciadv.aba4844.
Reitner, J.M., Ivy-Ochs, S., Drescher-Schneider, R., Hajdas, I., Linner, M., 2016. Reconsidering the current stratigraphy of the Alpine Lateglacial: implications of the sedimentary and morphological record of the Lienz area (Tyrol/Austria). E&G Quat. Sci. Jour. 65, 113–144. https://doi.org/10.3285/eg.65.2.02.
Sacco, F., 1925. Il glacialismo nelle Valli dell'Orco e della Soana. Boll. del Com. Glaciol. Ital. 6, 35–64.
Sacco, F., 1921a. Il glacialismo nel Gruppo del Gran Paradiso. Boll. del Com. Glaciol. Ital. 4, 121–168.
Sacco, F., 1921b. Il glacialismo nelle Valli Grisanche, Rhemes e Savaranche (Valle d'Aosta). L'Universo 11–12, 743–785.
Sailer, R., 2001. Späteiszeitliche Gletscherstände in der Ferwallgruppe (PhD Thesis). Universität Innsbruck.
Salvatore, M.C., Zanoner, T., Baroni, C., Carton, A., Banchieri, F.A., Viani, C., Giardino, M., Perotti, L., 2015. The state of Italian glaciers: a snapshot of the 2006-2007 hydrological period. Geogr. Fis. Din. Quaternaria 38, 175–198. https://doi.org/10.4461/GFDQ.2015.38.16.
Scapozza, C., Castelletti, C., Soma, L., Dall'Agnolo, S., Ambrosi, C., 2014. Timing of LGM and deglaciation in the southern Swiss Alps. Géomorphol. Relief, Process. Environ. 20, 307–322. https://doi.org/10.4000/geomorphologie.10753.
Schenk, F., Väliranta, M., Muschitiello, F., Tarasov, L., Heikkilä, M., Björck, S., Brandefelt, J., Johansson, A.V., Näslund, J.-O., Wohlfarth, B., 2018. Warm summers during the Younger Dryas cold reversal. Nat. Commun. 9, 1634. https://doi.org/10.1038/s41467-018-04071-5.
Scotti, R., Brardinoni, F., Crosta, G.B., Cola, G., Mair, V., 2017. Time constraints for

post-LGM landscape response to deglaciation in Val Viola, Central Italian Alps. Quat. Sci. Rev. 177, 10–33. https://doi.org/10.1016/j.quascirev.2017.10.011.
Spagnolo, M., Ribolini, A., 2019. glacier extent and climate in the Maritime Alps during the younger Dryas. Palaeogeogr. Palaeoclimatol. Palaeoecol. 536, 109400. https://doi.org/10.1016/j.palaeo.2019.109400.
Tabari, H., Willems, P., 2018. Lagged influence of Atlantic and Pacific climate patterns on European extreme precipitation. Sci. Rep. 8, 5748. https://doi.org/10.1038/s41598-018-24069-9.
Vanuzzo, C., 2001. The glacier retreat in Valle D'Aosta (Western Italian Alps) from the Little Ice Age to the second half of the 20th century: linear, areal, volumetric and equilibrium line altitute changes. Geogr. Fis. Din. Quaternaria 24, 99–113.
Višnjević, V., Herman, F., Prasicek, G., 2020. Climatic patterns over the European Alps during the LGM derived from inversion of the paleo-ice extent. Earth Planet Sci. Lett. 538, 116185. https://doi.org/10.1016/j.epsl.2020.116185.
Walker, I.R., Cwynar, L.C., 2006. Midges and palaeotemperature reconstruction—the North American experience. Quat. Sci. Rev. 25, 1911–1925. https://doi.org/10.1016/j.quascirev.2006.01.014.
Walker, I.R., Levesque, A.J., Cwynar, L.C., Lotter, A.F., 1997. An expanded surface-water palaeotemperature inference model for use with fossil midges from eastern Canada. J. Paleolimnol. 18, 165–178. https://doi.org/10.1023/A:1007997602935.
Wirsig, C., Zasadni, J., Christl, M., Akçar, N., Ivy-Ochs, S., 2016. Dating the onset of LGM ice surface lowering in the High Alps. Quat. Sci. Rev. 143, 37–50. https://doi.org/10.1016/j.quascirev.2016.05.001.
Zemp, M., Hoelzle, M., Haeberli, W., 2007. Distributed modelling of the regional climatic equilibrium line altitude of glaciers in the European Alps. Global Planet. Change 56, 83–100. https://doi.org/10.1016/j.gloplacha.2006.07.002.